

This is the peer reviewed version of the following article:

Consolidation of different hydroxyapatite powders by SPS: Optimization of the sintering conditions and characterization of the obtained bulk products / Cuccu, A.; Montinaro, S.; Orrù, R.; Cao, G.; Bellucci, Devis; Sola, Antonella; Cannillo, Valeria. - In: CERAMICS INTERNATIONAL. - ISSN 0272-8842. - 41:1 Part A(2015), pp. 725-736. [10.1016/j.ceramint.2014.08.131]

Terms of use:

The terms and conditions for the reuse of this version of the manuscript are specified in the publishing policy. For all terms of use and more information see the publisher's website.

06/05/2026 01:25

(Article begins on next page)

Manuscript Number: CERI-D-14-03417R1

Title: Consolidation of different Hydroxyapatite powders by SPS: optimization of the sintering conditions and characterization of the obtained bulk products

Article Type: Full Length Article

Keywords: Hydroxyapatite; Tri-Calcium Phosphate (TCP), Spark Plasma Sintering; Mechanical properties

Corresponding Author: Dr. Roberto Orru, PhD

Corresponding Author's Institution: University of Cagliari

First Author: Alessio Cuccu, PhD Student

Order of Authors: Alessio Cuccu, PhD Student; Selena Montinaro, PhD; Roberto Orru, PhD; Giacomo Cao, PhD; Devis Bellucci, PhD; Antonella Sola; Valeria Cannillo, PhD

Abstract: The difference in purity, particle size, microstructure, and thermo-chemical stability of three commercially available hydroxyapatite powders are found to play an important role during their consolidation using Spark Plasma Sintering (SPS) as well as strongly affect the characteristics of the resulting sintered bodies. A fully dense material without secondary phases was obtained by SPS at 900°C, when using the relatively small sized, with refined grains and high purity powders. The sintered product, consisting of sub-micrometer sized hydroxyapatite grains, displayed optical transparency and good mechanical properties. In contrast, the higher temperature levels (up to 1200 °C) needed to sinter powders with larger particles, or finer ones which contain additional phases, lead to products with coarser microstructures and/or significant amount of β -TCP as a result of HAp decomposition. Optical characteristics, hardness and elastic modulus of the resulting sintered samples are correspondingly worsened.

Replies to the Reviewer's comments

First of all we would like to thank the Reviewer for considering our manuscript very good and the related conclusions interesting.

As suggested by the Reviewer, the comparison of the transformation temperatures from HAp to beta-TCP of the commercial powders considered in the present work with those ones indicated in the literature is reported in the revised version of the manuscript along with the corresponding sources.

1 **Abstract**
2
3

4 The difference in purity, particle size, microstructure, and thermo-chemical
5 stability of three commercially available hydroxyapatite powders are found to play an
6 important role during their consolidation using Spark Plasma Sintering (SPS) as well as
7 strongly affect the characteristics of the resulting sintered bodies. A fully dense material
8 without secondary phases was obtained by SPS at 900°C, when using the relatively
9 small sized, with refined grains and high purity powders. The sintered product,
10 consisting of sub-micrometer sized hydroxyapatite grains, displayed optical
11 transparency and good mechanical properties.
12
13
14
15
16
17
18
19
20
21

22 In contrast, the higher temperature levels (up to 1200 °C) needed to sinter
23 powders with larger particles, or finer ones which contain additional phases, lead to
24 products with coarser microstructures and/or significant amount of β -TCP as a result of
25 HAp decomposition. Optical characteristics, hardness and elastic modulus of the
26 resulting sintered samples are correspondingly worsened.
27
28
29
30
31
32
33
34
35
36
37
38
39

40 *Keywords:* Hydroxyapatite; Tri-Calcium Phosphate (TCP), Spark Plasma Sintering;
41
42 Mechanical properties
43
44
45
46
47
48
49
50
51
52
53
54
55
56
57
58
59
60
61
62
63
64
65

1. Introduction

Since hydroxyapatite ($\text{Ca}_{10}(\text{PO}_4)_6(\text{OH})_2$), often referred to as HAp or HA, represents the main inorganic component of hard human tissues (bones and teeth), it is not surprising that it is regarded as one of the most investigated ceramics for biomedical application in either bulk form or as coating [1-3].

Due to its importance, a large number of research studies addressed to the fabrication of bulk HAp products using pressureless and pressure-assisted sintering methods, mainly conventional Hot Pressing (HP) or innovative Spark Plasma Sintering (SPS) techniques, have been conducted so far [2].

It is well known that one of the main concerns accompanying heat processing of HAp is related to its thermochemical instability [4]. Indeed, HAp decomposition takes place when relatively high temperature conditions are encountered during powder consolidation. Correspondingly, negative effects on mechanical and biological characteristics of the resulting materials are often produced.

In this context, the SPS technology offers a suitable method for obtaining bulk ceramic products under relatively milder sintering conditions [5]. Indeed, the electric pulsed current flowing directly through the die containing the non-conductive HAp powders permits sample heating at higher rates and in shorter processing times with respect to conventional HP, where external elements are employed as heating source.

Along these lines, several studies have been conducted in the literature in the last decade for the fabrication of dense HAp ceramics by SPS [6-19]. Most of them take advantage of the SPS technology for the consolidation of previously synthesized lab-made [6,8-11,13-15,17,19] or commercial [7,10,16,18-19] HAp powders. Alternatively,

1 one attempt to synthesize and simultaneously densify the HAp by reactive SPS was
2
3 carried out starting from $\text{CaHPO}_4 \cdot 2\text{H}_2\text{O}$ and $\text{Ca}(\text{OH})_2$ as reaction promoters [12].
4
5

6 As a consequence of the different starting materials, the operating conditions
7
8 (i.e. holding temperature, heating rate, applied pressure and dwell time) adopted in these
9
10 studies to obtain nearly full dense HAp-based bodies vary in a quite wide range, i.e.
11
12 700-1200°C. However, the potential benefits deriving from the use of SPS are
13
14 confirmed. In this regard, it is clear that the characteristics of the initial powders deeply
15
16 affect the final composition as well as the resulting mechanical and biological properties
17
18 of the sintered material. Indeed, the decomposition of HAp to produce Tri-Calcium
19
20 Phosphate (TCP) [8,11,15] could not be associated only to the more drastic SPS
21
22 conditions correspondingly adopted. For instance, no additional phases other than HAp
23
24 were found in the 99.7% dense material fabricated in 10 min by SPS at 1200°C [9]. On
25
26 the other hand, the presence of β -TCP was evidenced by Lee et al. [11] in the 96.4%
27
28 dense material obtained when the sintering process was conducted at 1000°C for 2 min.
29
30 The use of different SPS apparatuses and sample configurations might also play a role
31
32 in this regard.
33
34
35
36
37
38
39

40 In order to systematically investigate the influence of the characteristics of the
41
42 initial powders on the final composition as well as the resulting mechanical properties,
43
44 in the present work bulk HAp ceramics are produced by SPS using three different
45
46 commercially available powders. The starting materials are first characterized by laser
47
48 scattering analysis, X-ray diffraction (XRD), SEM, heat treatments in air and
49
50 thermogravimetric analysis in order to highlight their main differences (purity, particle
51
52 and crystallite size, thermochemical stability, etc.). Each HAp powder is then
53
54 consolidated by SPS. In particular, a systematic investigation is performed to identify
55
56
57
58
59
60
61
62
63
64
65

1 the optimal sintering temperatures to obtain fully dense products, while keeping all the
2
3 other parameters unchanged (SPS equipment, applied pressure, heating rate, holding
4
5 time, sample configuration). The resulting optimal samples are compared from the
6
7
8 compositional, microstructural and mechanical point of view.
9

10
11
12
13
14
15
16
17
18
19
20
21
22
23
24
25
26
27
28
29
30
31
32
33
34
35
36
37
38
39
40
41
42
43
44
45
46
47
48
49
50
51
52
53
54
55
56
57
58
59
60
61
62
63
64
65

2. Experimental materials and methods

The main characteristics, as provided by the vendors, of the three different commercial powders investigated in this work for the fabrication of dense HAp products are reported in **Table 1**. A more detailed particle size analysis was carried out in the present study taking advantage of a laser light scattering analyser (CILAS 1180, France). The starting powders were also examined by XRD using a Philips PW 1830 X-rays diffractometer equipped with a Ni filtered Cu K α radiation ($\lambda=1.5405$ Å). The powders' morphology was investigated by scanning electron microscopy (SEM, mod. S4000, Hitachi, Japan).

The thermal stability of the HAp powders was studied by heat treating the raw materials in air environment at different temperatures, in the range of 700-1250°C, using a laboratory furnace (Nabertherm, mod. N60/ER, Germany). In addition, a thermogravimetric analysis (TGA) under non-isothermal conditions was carried out by slowly heating (10°C/min) the initial powders from room temperature to 1450°C using a NETZSCH STA 409PC Simultaneous DTA-TGA Instrument in presence of 100 mL/min air flow.

The HAp powders were sintered in the form of cylindrical disks (about 15 mm diameter, 3 mm thickness) by Spark Plasma Sintering (SPS 515S model, Sumitomo Coal Mining Co Ltd) under vacuum conditions (20 Pa). This apparatus is based on the combination of a uniaxial press (50 kN) with a DC pulsed current generator (10 V, 1500 A, 300 Hz), thus simultaneously providing a pulsed electric current through the sample (when electrically conductive) and the graphite container, along with a mechanical pressure through the punches. The pulse cycle was set to 12 ms on and 2 ms off, being the characteristic time of single pulse equal to about 3.3 ms. Both the die and the

1 plungers were made of AT101 graphite (Atal s.r.l., Italy). The powders to be sintered
2
3 (about 1.6 g) were poured inside a cylindrical graphite die with outside diameter of 35
4
5 mm, inside diameter of 15 mm, and 30 mm high. To protect the die/plungers and make
6
7 sample release easier after sintering, the compact was lined with a graphite foil (0.13
8
9 mm thick, Alfa Aesar Karlsruhe, Germany). In addition, the die was surrounded by a
10
11 layer of graphite felt (3 mm thick, Atal s.r.l., Italy) for thermal insulation purpose.
12
13
14

15
16 The most important SPS parameters, i.e. temperature, current, voltage between
17
18 the machine electrodes, mechanical load and vertical sample displacement, were
19
20 recorded in real time. The displacement output provides an indication of the evolution
21
22 of the powders' densification during SPS. However, the thermal expansion of sample,
23
24 electrodes, graphite blocks, spacers and plungers is also responsible for the measured
25
26 value. All these contributions, but that of the sample, can be separately accounted for by
27
28 following a specific procedure [20], thus obtaining the sample shrinkage (δ), which will
29
30 be considered in what follows. In any case, the final consolidation level was determined
31
32 by measuring the density of the samples obtained at the end of the SPS process. After
33
34 sintering, the electric current was turned off, the mechanical load released, the sample
35
36 allowed to cool to room temperature and then removed from the die. For the sake of
37
38 reproducibility, each experiment was repeated at least twice.
39
40
41
42
43
44

45 SPS experiments were conducted under temperature controlled mode using a K-
46
47 type thermocouple (Omega Engineering Inc., USA) inserted inside a small hole drilled
48
49 near the center of the external surface of the graphite die. Temperature levels were also
50
51 measured by means of an infrared pyrometer (CHINO, mod. IR-AHS2, Japan) focused
52
53 on the lateral surface of the graphite mould.
54
55
56
57
58
59
60
61
62
63
64
65

1 The effect of the dwell temperature, T_D , on the product characteristics was
2
3 investigated by performing all SPS experiments at constant values of the holding time
4
5 ($t_D=5$ min), the mechanical pressure ($P=30$ MPa), and the heating rate ($75^\circ\text{C}/\text{min}$), to
6
7 achieve the desired value from the room temperature.
8
9

10 Relative densities were determined by the Archimedes' method after accurately
11
12 polishing SPSed products and considering $3.16\text{ g}/\text{cm}^3$ as theoretical value.
13
14

15 The microstructure of the optimal SPSed products was examined by SEM. To this
16
17 aim, the sintered specimens were first mirror polished and then chemically etched for 10
18
19 s using a 3 vol.% HNO_3 solution.
20
21

22 The selected samples were also investigated from a mechanical point of view. A
23
24 depth-sensing indentation technique was applied to determine the local elastic modulus
25
26 and Vickers micro-hardness. With this aim, the samples were cut, mounted in resin and
27
28 polished according to a standard metallographic procedure. The indentations were
29
30 performed using an OpenPlatform instrument (CSM Instruments, Peseux, Switzerland),
31
32 equipped with a Vickers indenter tip. For each sample, two different loading conditions
33
34 were considered:
35
36

37 - low load: maximum applied load: 0.50 N; loading/unloading rate: 0.75 N/min;
38
39 loading time: 15 s;
40
41

42 - high load: maximum applied load: 2.00 N; loading/unloading rate: 3.00 N/min;
43
44 loading time: 15 s.
45
46

47 For statistical purposes, 30 indentations were performed for each sample and for each
48
49 loading condition. For each indentation, the load-penetration depth curve was
50
51 automatically acquired and then analyzed according to the Oliver and Pharr method to
52
53 evaluate the local elastic properties [21].
54
55
56
57
58
59
60
61
62
63
64
65

1 **3. Results and discussion**

2
3 **3.1 Characterization of initial powders**

4
5
6 The results related to the granulometry of the three different types of powders
7
8 measured by laser light scattering analysis are summarized in **Table 2**. While **HAp_1**
9
10 and **HAp_2** systems display similar fine particles, **HAp_3** powders are relatively
11
12 coarser. This feature is clearly confirmed when examining the corresponding SEM
13
14 micrographs (**Figure 1**). Specifically, both **HAp_1** and **HAp_2** materials generally
15
16 consist of micrometer-sized aggregates made of sub-micrometer grains. In contrast, the
17
18 **HAp_3** product exhibits coarser particles, up to 100 μm sized, characterized by a
19
20 sponge like structure with pores down to 100 nm (**Figure 1(f)**).
21
22
23
24

25 The comparison of the corresponding XRD patterns is shown in **Figure 2**. On the
26
27 basis of this analysis it is possible to state that HAp is the only phase present in **HAp_2**
28
29 and **HAp_3**, while a non-negligible amount of CaHPO_4 was detected in **HAp_1**
30
31 powders. In addition, the **HAp_1** and **HAp_2** systems displayed relatively broad
32
33 diffraction peaks, to indicate their finer microstructure, in contrast to the narrow peaks
34
35 observed when considering the **HAp_3** material.
36
37
38
39

40 The thermal stability of the starting powders was first evaluated by heat-treating
41
42 the different raw materials in a furnace under air environment. The XRD spectra of the
43
44 heat-treated powders are reported in **Figures 3(a)-(c)**.
45
46

47 No additional phases were detected by XRD when the **HAp_1** system was heat-
48
49 treated at temperatures equal or lower than 700°C. On the other hand, as the
50
51 temperature was raised to 750°C, the β -TCP phase (rhombohedral lattice) appeared in
52
53 the XRD pattern of the end product. In addition, as higher thermal levels were achieved,
54
55 the decomposition of HAp was found to increase progressively. Specifically, β -TCP
56
57
58
59
60
61
62
63
64
65

1 becomes the major crystalline constituent in powders heat treated at 900°C, while only
2
3
4 minor amounts of HAp and CaHPO₄ are present.

5
6 On the other hand, as evidenced in **Figures 3(b)** and **3(c)**, no secondary species
7
8 are found in XRD patterns of **HAp_2** and **HAp_3** powders heat-treated up to 1250°C.
9
10 The most significant change, particularly for **HAp_2**, is represented by a certain peak
11
12 narrowing, with respect to the original material, thus indicating that grain growth is
13
14 induced by the heat treatment.
15
16

17
18 In order to overcome the temperature limitation (1300°C) of the furnace utilized
19
20 in the previous heat-treatment as well as to obtain further information regarding the
21
22 chemico-physical stability of the powders under consideration, the latter ones have been
23
24 also characterized by TGA up to 1450°C. The corresponding mass losses as a function
25
26 of the temperature are plotted in **Figure 4** for the three systems. It is possible to observe
27
28 that only for temperatures above 1000°C the **HAp_3** material significantly changes its
29
30 mass. In contrast, the curves corresponding to the other two products markedly decrease
31
32 just after the TGA test starts. Moreover, the weight losses resulting at the end of the
33
34 experiment for **HAp_1** and **HAp_2** are 3-4 times higher than the value obtained when
35
36 processing the **HAp_3** material.
37
38
39
40
41

42
43 The mass loss profiles described above can be associated to the compositional
44
45 changes taking place in the powders as the temperature increases during the TGA test.
46
47 This information was obtained by interrupting the experiments at different time
48
49 intervals corresponding to the arrows indicated in **Figure 4** and analyzing by XRD the
50
51 related products. The obtained results are shown in **Figure 5(a)-5(c)**. As far as the
52
53 **HAp_1** is concerned, it is seen that the formation of β -TCP is evidenced at relatively
54
55 low temperature (500°C), i.e. immediately after the sudden slope change manifested by
56
57
58
59
60
61
62
63
64
65

1 the mass loss curve (**Figure 4**). Nevertheless, the corresponding sample weight loss
2
3 could be mostly ascribed to the occurrence of dehydroxylation phenomena.
4

5
6 The XRD analysis performed when the TGA test for the **HAp_1** system was
7
8 conducted at 1250°C indicated that a complete decomposition of HAp to β -TCP
9
10 occurred. Minor amounts of CaHPO_4 , originally present in the raw material, were also
11
12 found at this stage. Furthermore, as the thermal analysis was prolonged to 1450°C, it is
13
14 possible to observe a significant conversion of TCP from the β to the α (monoclinic)
15
16 form, which represents the thermodynamically stable phase at high temperatures. This
17
18 outcome is consistent with the fact that the transformation of β -TCP into the α - form is
19
20 commonly reported to occur at temperatures above 1120-1170°C [2].
21
22
23
24

25 In contrast, as evidenced in **Figure 4(b)**, no additional peaks are detected in XRD
26
27 patterns of the **HAp_2** product subjected to TGA at 1250°C. This feature clearly
28
29 confirms its higher thermal stability with respect to the **HAp_1** system. Therefore, the
30
31 significant weight loss (about 7%) observed at 1250°C for this system (**Figure 4**) can be
32
33 only associated to the dehydroxylation of HAp. Nevertheless, a completely different
34
35 situation is encountered when the temperature is raised to 1450°C. Indeed, a
36
37 considerable amount of TCP, particularly in its α - form, is present in the end product
38
39 along with residual HAp.
40
41
42
43
44

45 A behavior qualitatively similar to that described for **HAp_2** was also displayed
46
47 by the **HAp_3** material, which also exhibited a relatively high thermal stability.
48
49 Specifically, as shown in **Figure 5(c)**, HAp was the only phase found by XRD in
50
51 powders subjected to TGA at 1250°C. In addition, it should be noted that the amount of
52
53 α - and β -TCP formed when the temperature was increased to 1450°C is even lower with
54
55 respect to that found in the **HAp_2** material.
56
57
58
59
60
61
62
63
64
65

1 In conclusion, on the basis of the results obtained when heat treating in air the
2 three HAp systems, **HAp_1** powders is found to display a marked thermal instability as
3 HAp decomposes at rather low temperatures. In contrast, when the **HAp_2** and **HAp_3**
4 HAp decomposes at rather low temperatures. In contrast, when the **HAp_2** and **HAp_3**
5 powders are heat-treated in air flow, the transformation of HAp takes place only at
6 temperatures above 1250°C to produce TCP, particularly in its α - configuration.
7 Furthermore, the significant weight loss displayed by **HAp_1** and **HAp_2** in
8 comparison to **HAp_3** could be likely associated to their relatively larger surface area
9 due to the corresponding finer particles size, so that the occurrence of dehydroxylation
10 phenomena is facilitated.
11
12
13
14
15
16
17
18
19
20
21

22
23 **As far as the different thermal stability exhibited by the three HAp powders**
24 **under examination is concerned, it should be noted that the minimum temperature**
25 **to which calcium phosphate apatites decompose is well known to depend on several**
26 **factors such as powders purity, particles size and shape, Ca/P molar ratio, as well**
27 **as the environmental conditions under which the heat treatment is carried out [4;**
28 **22-24]. Thus, the decomposition of HAp to β -TCP taking place at relatively low**
29 **temperature for the case of HAp_1 system can be readily ascribed to the presence**
30 **of secondary phases (CaHPO_4) in the corresponding starting powders. In addition,**
31 **the transformation temperature of about 750°C found in this case during heat**
32 **treatment experiments in air furnace (cf. Figure 3a) is in agreement with Graeve et**
33 **al. [24] findings. Specifically, in the latter study, no indication of compositional**
34 **changes was evidenced by XRD after powder calcination at 600°C, whereas β -TCP**
35 **was clearly detected at 800°C. A dissociation temperature of HAp to β -TCP of**
36 **about 700°C was also reported in the literature relatively to heat-treated calcium**
37 **phosphate apatites with $1.5 < \text{Ca/P} < 1.667$ [23]. The fact that during the TGA**
38
39
40
41
42
43
44
45
46
47
48
49
50
51
52
53
54
55
56
57
58
59
60
61
62
63
64
65

1 experiments conducted in the present study, β -TCP was already detected at 500°C
2
3 (cf. Figure 5a) might be likely due to the air flow conditions adopted during this
4
5 analysis which, apparently, are able to anticipate HAp decomposition.
6
7

8 Differently from the HAp_1 system, the characteristics of HAp_2 and HAp_3
9
10 powders, particularly their relatively higher purity, make them more thermally
11
12 stable. In this regard, it should be noted that the temperature levels (above
13
14 1250°C) at which HAp was found to decompose to α -TCP (cf. Figures 3 and 5) are
15
16 also well in agreement with the interval of 1350-1400°C reported in the literature
17
18 on this subject [4; 22].
19
20
21
22
23
24

25 3.2 Powders consolidation by SPS

26
27 Typical outputs of sample shrinkage (δ) and temperature obtained during the
28
29 densification process by SPS of HAp powders are reported in **Figure 6** for the case of
30
31 the **HAp_2** system. Specifically, these data refer to the conditions of $T_D=900$ °C, 75
32
33 °C/min heating rate, $t_D=5$ min, and $P=30$ MPa. Only minor changes in the sample
34
35 shrinkage are observed during the first 9 min of the SPS process, i.e. for temperatures
36
37 below 700°C. On the other hand, as the temperature is raised above that level, the slope
38
39 of the sintering curve rapidly increases approximately at a constant rate to reach a
40
41 sample shrinkage of about 4 mm when the dwell temperature is achieved. Afterwards,
42
43 the δ parameter modestly varies up to the end of the SPS experiment. Analogous
44
45 qualitative comments can be made when examining the sintering behavior of the other
46
47 systems and/or consolidation conditions investigated.
48
49
50
51
52
53

54
55 The effect of the dwell temperature on SPSed product density is shown in
56
57 **Figure 7** for the different HAp materials taken into account in the present work. All the
58
59
60
61
62
63
64
65

1 plotted data refer to sintering experiments conducted at 30 MPa, $t_D=5$ min and 75
2
3 °C/min heating rate. As expected, the sample densification is improved as the sintering
4
5 temperature is increased, although the three processed powders displayed a quite
6
7 different behavior. Indeed, while the **HAp_2** material achieved a high consolidation
8
9 level at 800°C, the density values obtained by the other two materials, when processed
10
11 under the same conditions, are still extremely low. In particular, the temperature
12
13 condition required to produce fully dense **HAp_2** samples is 900°C, whereas the
14
15 optimal temperature to achieve the same goal when starting from **HAp_3** powders is
16
17 1200°C. A peculiar behavior is observed when optimizing the sintering process for the
18
19 **HAp_1** system. Specifically, a significant sample densification was evidenced in the
20
21 range of 800-900°C, while a further temperature increase was accompanied only by a
22
23 slight change in product density and the theoretical density value of 3.16 g/cm³ was not
24
25 achieved even at 1200°C.
26
27
28
29
30
31

32
33 The comparison of the XRD patterns of the original powders with the
34
35 corresponding SPS products obtained under optimal sintering conditions is shown in
36
37 **Figures 8(a)-8(c)** for the three systems.
38
39

40 As far as the **HAp_1** system is concerned, the first evidence of TCP formation is
41
42 observed at 700°C, i.e. when the sample is less than 50% dense (**Figure 7**). Moreover,
43
44 an increase of the temperature level up to 800°C is accompanied by a marked
45
46 decomposition of HAp to β -TCP, which becomes the major phase in the SPS product.
47
48 The amount of HAp tends to disappear when the sintering temperature is increased to
49
50 1200°C, and the corresponding material consists mainly of β -TCP. Minor amounts of
51
52 CaHPO₄ are still detected, as in the related starting powders. Thus, the fact that the
53
54 density of the SPSed product for the **HAp_1** system does not reach the theoretical value
55
56
57
58
59
60
61
62
63
64
65

1 of pure HAp (**Figure 7**) can be readily ascribed to the compositional changes of the
2
3 processing sample during SPS.
4

5
6 In contrast to the behavior described above for the **HAp_1** material and in
7
8 agreement with the results obtained with the heat-treatment of raw powders, the other
9
10 two systems exhibit a higher thermochemical stability during SPS. Indeed, regardless
11
12 the different dwell temperatures required to obtain fully dense materials, **Figures 8(b)**
13
14 and **8(c)** clearly indicate that no secondary phases are found by XRD in the fully dense
15
16 **HAp_2** and **HAp_3** samples, respectively.
17
18

19
20 Interesting information in this regard can be also obtained when examining the
21
22 gas pressure evolution inside the SPS chamber during the consolidation process. It
23
24 should be noted that a vacuum pump operates continuously to maintain the pressure
25
26 level in the sintering vessel at about 20 Pa. As shown in **Figure 9**, where the recorded
27
28 pressure data are plotted as a function of the SPS time, a completely different behavior
29
30 is exhibited by the three systems undergoing sintering. As far as the **HAp_1** and **HAp_2**
31
32 powders are concerned, it is seen that after about 2.5 min, i.e. when the measured
33
34 temperature was just above 200°C, the pressure value increased rapidly from the initial
35
36 value to approximately 40 Pa. This fact can be associated to the beginning of
37
38 dehydroxylation phenomena for both systems. However, for the case of **HAp_1**, an
39
40 additional sudden increase in the pressure level was observed at about 7 min. This event
41
42 began when the measured temperature was of about 500°C and can be ascribed to the
43
44 initial transformation $\text{HAp} \rightarrow \beta\text{-TCP}$. Indeed, the XRD analysis relative to TGA samples
45
46 (**Figure 5(a)**) evidenced the incipient presence of $\beta\text{-TCP}$ at 500°C. In addition, it is
47
48 important to note that when considering the **HAp_1** material, a relatively high pressure
49
50 level is observed during the entire duration of the consolidation process, thus providing
51
52
53
54
55
56
57
58
59
60
61
62
63
64
65

1 an indication of the progress of the hydroxyapatite decomposition. This fact is
2 confirmed by the XRD analysis of the corresponding specimen (**Figure 8(a)**). On the
3 other hand, during the sintering of **HAp_2** powders, the gas pressure first increases, as
4 mentioned above, then slightly decreases and finally drops down to the initial level at
5 about 12 min. On the basis of the XRD analysis results discussed previously, it is
6 possible to state that the change in gas pressure for the **HAp_2** system can be only due
7 to water losses. In addition, the fact that no gas expulsion from the sample is evidenced
8 during the isothermal stage at 900°C, allows us to conclude that dehydroxylation
9 phenomena correspondingly cease to occur.

10
11 In contrast to the previous finding, when the **HAp_3** powders are taken into
12 account, the sudden pressure increase is observed only for a relatively longer sintering
13 time, i.e. at about 12.5 min, when temperature levels above 1000°C are achieved. This
14 outcome, which is consistent with the results obtained by TGA (**Figure 4**) as well as
15 with the corresponding sample composition, still confirms its high thermochemical
16 stability with respect to **HAp_1** and **HAp_2**.

17
18 **Figures 10(a)-10(c)** show three SEM micrographs of the sintered products
19 obtained by SPS under optimal conditions, after being etched with a HNO₃ solution, as
20 described in the Experimental section. First of all, it is seen that the **HAp_1** system,
21 mostly consisting of 1-3 μm sized grains of β-TCP (**Figure 10(a)**), appears to be more
22 sensitive, as compared to the other competitive material, to the chemical etching
23 treatment. This feature provides an indication of the fact that HAp decomposition leads
24 to a material which is relatively less resistant to aggressive environments. In addition, it
25 is clear that a relatively finer microstructure, with respect to the other systems, is
26 obtained in **HAp_2** products, as demonstrated by the corresponding sub-micrometer

1 sized hydroxyapatite grains evidenced by the SEM micrograph shown in **Figure 10(b)**.
2
3 In contrast, the sintered **HAp_3** specimen is made of relatively coarser HA grains, up to
4
5 1-3 μm in size. Such differences in the microstructure of the bulk products can be
6
7 readily ascribed to the characteristics of the original powders as well as to the relatively
8
9 milder sintering conditions required when processing **HAp_2** powders (**Figure 7**).

10
11
12
13 Three optical photos corresponding to optimal dense samples, about 2.4 mm
14
15 thick, of the investigated HAp systems are reported in **Figures 11(a)-11(c)**. The product
16
17 which displays a relatively higher transparency is **HAp_2** followed by **HAp_3**, whereas
18
19 **HAp_1** appears to be the most opaque material. Such finding is consistent with the
20
21 results described above. Indeed, the **HAp_2** system is obtained from the relatively more
22
23 refined starting powders and no HAp decomposition was detected during the
24
25 consolidation process. On the other hand, the lack of transparency in the SPSed sample
26
27 obtained using **HAp_1** powders could be likely associated to the significant chemical
28
29 transformations taking place during SPS (**Figure 8(a)**). Finally, although no secondary
30
31 phases have been detected in the sintered **HAp_3** specimen, its relatively coarse
32
33 microstructure could be responsible for the corresponding lower transparency.
34
35
36
37
38
39
40
41

42 **3.3 Mechanical characterization**

43
44 The impressions produced at 0.5 N load and 2.0 N load are exemplified in
45
46 **Figure 12(a)** and **Figure 12(b)**, respectively. In particular, such micrographs were
47
48 acquired on the cross section of the **HAp_2** samples, but analogous indents were
49
50 induced and observed also on the other materials.
51
52
53

54 As shown in **Figure 13(a)**, the micro-hardness of the HAp sintered bodies
55
56 slightly decreases when the applied load rises from 0.5 to 2.0 N, as a result of the well-
57
58
59
60
61
62
63
64
65

1 known Indentation Size Effect (ISE) [22][25]. The local elastic modulus, instead, is less
2
3 sensitive to the applied load, especially for the **HAp_1** and **HAp_2** samples, as shown
4
5 in **Figure 13(b)**. Independently of the applied load, the best local mechanical properties
6
7 are achieved by the **HAp_2** sintered bodies, a result that is reasonable on the basis of
8
9 the mineralogical composition and compact microstructure detected for this material, as
10
11 described in the previous paragraphs. The relatively low mechanical properties observed
12
13 for the **HAp_1** samples with respect to the other two SPSeD HAp materials are probably
14
15 due to the chemical transformations occurred during sintering and the incomplete
16
17 densification. However, it is worth noting that, also for the **HAp_1** samples, the
18
19 hardness is well comparable to that usually reported in the literature for apatites
20
21 produced with different methods. Ramesh et al. [23][26], for example, analyze the
22
23 sintering properties of hydroxyapatite powders obtained with different methods and
24
25 describe hardness values indicatively in the 50-700 HV range, whereas Curran et al.
26
27 [24][27], comparing undoped and Sr-doped sintered HAp samples treated at 1200°C,
28
29 find values in the 200-500 HV range. Also the local elastic modulus matches the values
30
31 commonly observed for crystalline apatite solids (e.g. 114 GPa according to the
32
33 classical study of **Gilmore et al.** [25][28]).
34
35
36
37
38
39
40
41
42
43
44

45 **4. Summary and concluding remarks**

46
47 Three commercially available HAp powders are processed in this work taking
48
49 advantage of the Spark Plasma Sintering technology to rapidly obtain nearly full dense
50
51 ceramics.
52
53

54
55 The starting powders differences in term of purity, particle size, microstructure,
56
57 and thermo-chemical stability are found to strongly affect their sintering behavior as
58
59
60
61
62
63
64
65

1 well as the characteristics of the resulting bulk materials. In particular, a fully dense
2 product with no secondary phases was obtained by SPS at 900°C when using the
3 relatively small sized, with refined grains and high purity **HAp_2** powders. On the other
4 hand, significantly higher temperature levels (1200 °C) are required to eliminate
5 residual porosity in the product when starting from the coarser **HAp_3** powders.
6 Nevertheless, such temperature conditions are not so drastic to induce the formation of
7 undesired phases in this material during its consolidation by SPS. In contrast, a marked
8 decomposition of HAp to β -TCP, which becomes the major phase in the end product,
9 was obtained under the same conditions (1200°C) when processing the **HAp_1** system,
10 whose initial fine powders also contained CaHPO₄.
11
12
13
14
15
16
17
18
19
20
21
22
23
24

25 The optical, microstructural, and mechanical properties of the obtained dense
26 bodies are consistent with the characteristics of the starting material and the
27 corresponding SPS conditions adopted. The system exhibiting relatively higher
28 transparency is **HAp_2** whereas the other specimens, particularly **HAp_1**, appear more
29 opaque. This outcome is important as sample transparency enables direct viewing of
30 living cells during biological characterization by light microscopy of the obtained
31 materials. The achieved samples transparency can be directly associated with the related
32 microstructures. Indeed, a **HAp_2** product consisting of sub-micrometer sized
33 hydroxyapatite grains was obtained after the consolidation process, while relatively
34 coarser microstructures were evidenced in the **HAp_1** and **HAp_3** end products. In
35 addition, the transformation HAp \rightarrow β -TCP occurred during sintering makes **HAp_1**
36 more sensitive to the chemical etching with respect to the other systems where the
37 decomposition above was avoided.
38
39
40
41
42
43
44
45
46
47
48
49
50
51
52
53
54
55
56
57
58
59
60
61
62
63
64
65

1 As far as the mechanical properties of the three HAp materials are concerned, it
2
3 was found that they are well comparable to those ones generally reported in the
4
5 literature for apatite based products fabricated via alternative methods. In particular, the
6
7 best local mechanical properties are achieved by the **HAp_2** materials, whereas
8
9 relatively lower hardness and elastic modulus values were obtained for the **HAp_1**
10
11 samples. The good mechanical characteristics of the **HAp_2** material can be ascribed to
12
13 its thermal stability and finer microstructure. On the other hand, the presence of
14
15 significant amount of β -TCP in the **HAp_1** sintered product is, along with the
16
17 corresponding coarser microstructure, responsible for mechanical properties worsening.
18
19
20
21
22
23
24

25 **Acknowledgements**

26
27 The financial support for this work from Regione Autonoma della Sardegna
28
29 (Italy), L.R. n.7/2007, CUP n. F71J11001070002, is gratefully acknowledged. One of us
30
31 (A.C.) has performed his activity in the framework of the PhD in Biomedical
32
33 Engineering at the University of Cagliari, Italy. The authors thank Dr. Luca Desogus
34
35 (University of Cagliari, Italy) for his valuable support during the experimental activity.
36
37
38
39
40
41
42
43
44
45
46
47
48
49
50
51
52
53
54
55
56
57
58
59
60
61
62
63
64
65

References

- [1] Dorozhkin S.V. Bioceramics of calcium orthophosphates. *Biomaterials* 2010; 31(7): 1465-1485
- [2] Champion E. Sintering of calcium phosphate bioceramics. *Acta Biomater.* 2013; 9(4): 5855-5875
- [3] Bolelli G., Bellucci D., Cannillo V., Lusvarghi L., Sola A., Stiegler N., Müller P., Killinger A., Gadow R., Altomare L., De Nardo L. Suspension thermal spraying of hydroxyapatite: Microstructure and in vitro behaviour. *Mat. Sci. Eng. C* 2014; 34: 287-303.
- [4] Cihlar J., Buchal A., Trunec M. Kinetics of thermal decomposition of hydroxyapatite bioceramics. *J. Mater. Sci.* 1999; 34: 6121–6131
- [5] Orrù R., Licheri R., Locci A.M., Cincotti A., Cao G. Consolidation/synthesis of materials by electric current activated/assisted sintering. *Mat. Sci. Eng. R* 2009; 63(4-6): 127-287.
- [6] Gu Y.W., Loh N.H., Khor K.A., Tor S.B., Cheang P. Spark plasma sintering of hydroxyapatite powders. *Biomaterials* 2002; 23(1): 37-43
- [7] Nakahira A., Tamai M., Aritani H., Nakamura S., Yamashita K. Biocompatibility of dense hydroxyapatite prepared using an SPS process. *J. Biomed. Mater. Res.* 2002; 62(4): 550-557.
- [8] Kumar R., Cheang P., Khor K.A. Spark plasma sintering and in vitro study of ultra-fine HA and ZrO₂-HA powders. *J. Mater. Process. Technol.* 2003; 140: 420-425
- [9] Watanabe Y., Ikoma T., Monkawa A., Suetsugu Y., Yamada H., Tanaka J., Moriyoshi Y. Fabrication of transparent hydroxyapatite sintered body with high

- 1 crystal orientation by pulse electric current sintering. J. Amer. Ceram. Soc. 2005;
2
3 88(1): 243-245
4
5
6 [10] Guo X., Xiao P., Liu J., Shen Z. Fabrication of nanostructured hydroxyapatite via
7
8 hydrothermal synthesis and spark plasma sintering. J. Amer. Ceram. Soc. 2005;
9
10 88: 1026-1029
11
12
13 [11] Lee B.T., Shin N.Y., Han J.K., Song H.Y. Microstructures and fracture
14
15 characteristics of spark plasma-sintered HAp-5 vol.% Ag composites. Mat. Sci.
16
17 Eng. A 2006; 429(1-2): 348-352
18
19
20 [12] Omori M., Onoki T., Hashida T., Okubo A., Murakami Y. Low temperature
21
22 synthesis of hydroxyapatite from $\text{CaHPO}_4 \cdot 2\text{H}_2\text{O}$ and $\text{Ca}(\text{OH})_2$ based on effect of
23
24 the spark plasma system (SPS). Ceram. Int. 2006; 32(6): 617-621
25
26
27 [13] Guo X., Gough J.E., Xiao P., Liu J., Shen Z. Fabrication of nanostructured
28
29 hydroxyapatite and analysis of human osteoblastic cellular response. J Biomed
30
31 Mater Res A. 2007; 82(4):1022-1032.
32
33
34 [14] Li H., Khor K.A., Chow V., Cheang P. Nanostructural characteristics, mechanical
35
36 properties, and osteoblast response of spark plasma sintered hydroxyapatite. J
37
38 Biomed Mater Res A. 2007; 82(2): 296-303.
39
40
41 [15] Xu J.L., Khor K.A., Kumar R. Physicochemical differences after densifying radio
42
43 frequency plasma sprayed hydroxyapatite powders using spark plasma and
44
45 conventional sintering techniques. Mat. Sci. Eng. A 2007; 457(1-2): 24-32
46
47
48 [16] Gandhi A.A., Gunning R.D., Ryan K.M., Tofail S.A.M. The role of texturing and
49
50 densification on optical transmittance of hydroxyapatite ceramics. J. Amer.
51
52 Ceram. Soc. 2010; 93(11): 3773-3777.
53
54
55
56
57
58
59
60
61
62
63
64
65

- 1 [17] Eriksson M., Liu Y., Hu J., Gao L., Nygren M., Shen Z. Transparent
2 hydroxyapatite ceramics with nanograin structure prepared by high pressure spark
3 plasma sintering at the minimized sintering temperature. J. Eur. Ceram. Soc.
4 2011; 31 (9): 1533-1540
5
6
7
8
9
- 10 [18] Liu Y., Shen Z. Dehydroxylation of hydroxyapatite in dense bulk ceramics
11 sintered by spark plasma sintering. J. Eur. Ceram. Soc. 2012; 32(11): 2691-2696.
12
13
14
- 15 [19] Kim B.N., Prajatelista E., Han Y.H., Son H.W., Sakka Y., Kim S. Transparent
16 hydroxyapatite ceramics consolidated by spark plasma sintering Scripta Mater.
17 2013; 69(5): 366-369
18
19
20
21
22
- 23 [20] Locci A.M., Orrù R., Cao G., Munir Z.A. Effect of ball milling on simultaneous
24 spark plasma synthesis and densification of TiC-TiB₂ composites. Mat. Sci. Eng.
25 A 2006; 434(1-2): 23-29.
26
27
28
29
- 30 [21] Oliver W.C., Pharr G.M. An Improved Technique for Determining Hardness and
31 Elastic Modulus using Load and Displacement Sensing Indentation Experiments.
32 J. Mater. Res. 1992; 7(6): 1564-1583.
33
34
35
36
- 37 [22] **Liao, C.-J., Lin, F.-H., Chen, K.-S., Sun, J.-S. Thermal decomposition and**
38 **reconstitution of hydroxyapatite in air atmosphere. Biomaterials 1999;**
39 **20(19): 1807-1813.**
40
41
42
43
44
- 45 [23] **Raynaud, S., Champion, E., Bernache-Assollant, D., Thomas, P. Calcium**
46 **phosphate apatites with variable Ca/P atomic ratio I. Synthesis,**
47 **characterisation and thermal stability of powders. Biomaterials 2002; 23(4):**
48 **1065-1072.**
49
50
51
52
53
54
55
56
57
58
59
60
61
62
63
64
65

1 [24] Graeve, O.A., Kanakala, R., Madadi, A., Williams, B.C., Glass, K.C.
2
3 Luminescence variations in hydroxyapatites doped with Eu²⁺ and Eu³⁺ ions.
4
5 Biomaterials 2010; 31(15): 4259-4267
6
7

8 [22][25] Milman Yu.V., Golubenko A.A., Dub S.N. Indentation size effect in
9
10 nanohardness. Acta Mater. 2011; 59(20): 7480-7487.
11
12

13 [23][26] Ramesh S., Aw K.L., Tolouei R., Amiriyan M., Tan C.Y., Hamdi M.,
14
15 Purbolaksono J., Hassan M.A., Teng W.D. Sintering properties of hydroxyapatite
16
17 powders prepared using different methods. Ceram. Int. 2013; 39: 111-119.
18
19

20 [24][27] Curran D.J., Fleming T.J., Towler M.R., Hampshire S. Mechanical
21
22 parameters of strontium doped hydroxyapatite sintered using microwave and
23
24 conventional methods. J. Mech. Behav. Biomed. Mater. 2011; 4(8): 2063-2073.
25
26

27 [25][28] Gilmore R.S., Katz J.L. Elastic properties of apatites. J. Mater. Sci. 1982;
28
29 17(4): 1131-1141.
30
31
32
33
34
35
36
37
38
39
40
41
42
43
44
45
46
47
48
49
50
51
52
53
54
55
56
57
58
59
60
61
62
63
64
65

Table 1. Starting powders characteristics as provided by suppliers.

System ID	Supplier/Code	Particle size (μm)	Compositional details
HAp_1	Sigma-Aldrich Cod. 21223	25-45 (average)	$\geq 90\%$ purity (KT as $\text{Ca}_3(\text{PO}_4)_2$)
HAp_2	Alfa-Aesar Cod. 36731	< 44	Calcium phosphate tribasic, 38.1% Ca
HAp_3	Plasma Biotol Ltd Cod. CAPTAL 60-1	$d_{10} = 21.7$ $d_{50} = 43$ $d_{90} = 77.8$	Hydroxyapatite, Whitlockite ($< 1\%$)

Table 2. Particle size characteristics of starting powders as determined by laser light scattering analyser.

System ID	d_{10} (μm)	d_{50} (μm)	d_{90} (μm)	Average size (μm)
HAp_1	1.2	4.9	17.2	7.1
HAp_2	1.3	5.1	13.4	6.3
HAp_3	8.8	34.0	52.0	32.7

Captions for figures

1 **Figure 1.** SEM images at different magnitudes of the initial HAp powders used in the present
2 investigation: (a)-(b) **HAp_1**, (c)-(d) **HAp_2** and (e)-(f) **HAp_3**.
3

4 **Figure 2.** XRD patterns on the initial HAp powders used in the present work: (a) **HAp_1**, (b)
5 **HAp_2** and (c) **HAp_3**.
6

7 **Figure 3.** Effect of the heat treatment in air on the composition of (a) **HAp_1**, (b) **HAp_2** and (c)
8 **HAp_3** powders.
9

10 **Figure 4.** Mass loss of HAp powders during TGA in air.
11

12 **Figure 5.** Compositional changes of (a) **HAp_1**, (b) **HAp_2** and (c) **HAp_3** powders during TGA
13 (10°C/min) in air (100 ml/min).
14

15 **Figure 6.** Temperature and sample shrinkage time profiles recorded during consolidation of
16 **HAp_2** powders by SPS (900°C, 75 °C/min, $t_D=5$ min, 30 MPa).
17

18 **Figure 7.** Influence of the sintering temperature on the density of the HAp products obtained by
19 SPS (75 °C/min, $t_D=5$ min, 30 MPa).
20

21 **Figure 8.** Comparison of XRD patterns before and after consolidation by SPS (75 °C/min, $t_D=5$
22 min, 30 MPa) of (a) **HAp_1**, (b) **HAp_2** and (c) **HAp_3** powders.
23

24 **Figure 9.** Temporal evolution of gas pressure during the SPS process (75 °C/min, $t_D=5$ min, 30
25 MPa) of **HAp_1**, **HAp_2** and **HAp_3** powders.
26

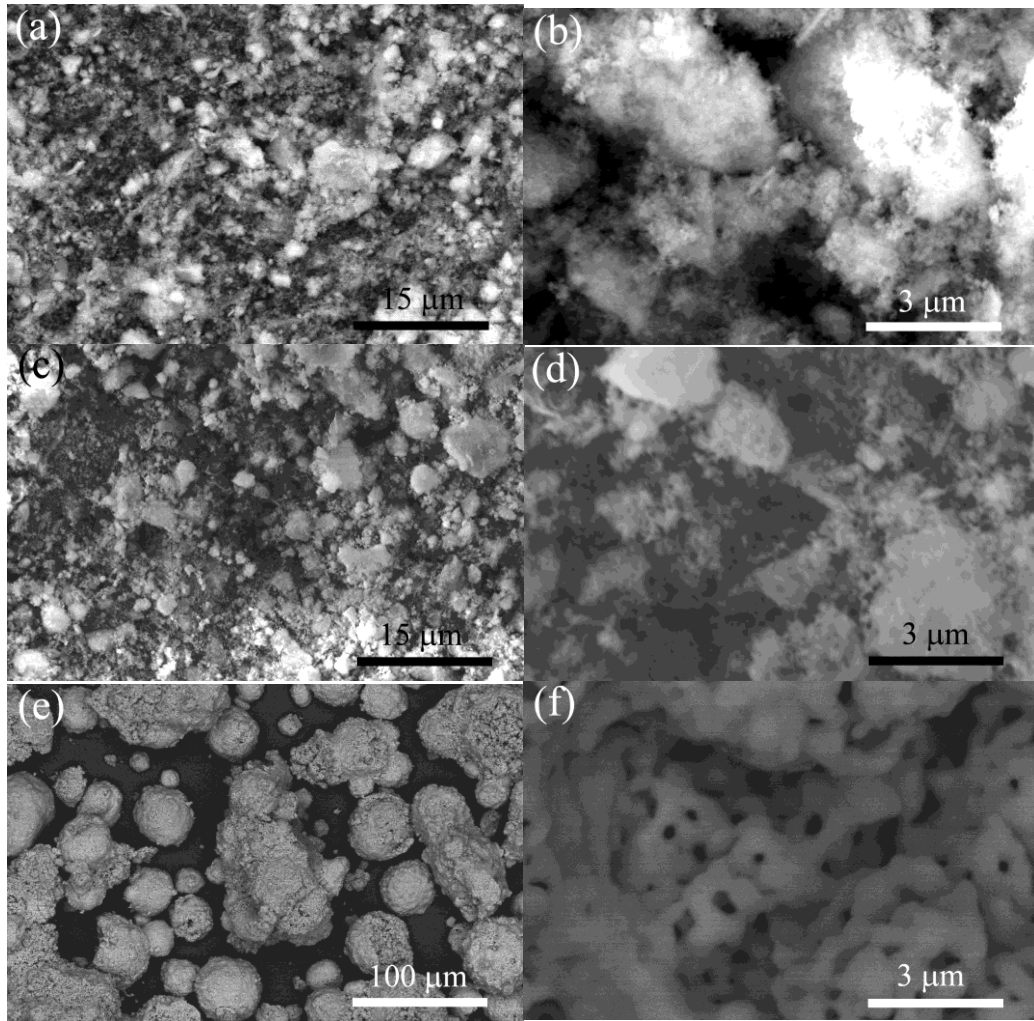
27 **Figure 10.** SEM micrographs (10000 x) of chemically etched dense products obtained by SPS
28 under optimal conditions: (a) **HAp_1**, (b) **HAp_2** and (c) **HAp_3**.
29

30 **Figure 11.** Optical photographs of dense products obtained by SPS under optimal conditions: (a)
31 **HAp_1**, (b) **HAp_2** and (c) **HAp_3**.
32

33 **Figure 12.** Residual imprints produced in the cross section of the **HAp_2** samples during
34 indentation tests: (a) 0.5 N and 2.0 N (b) loads.
35

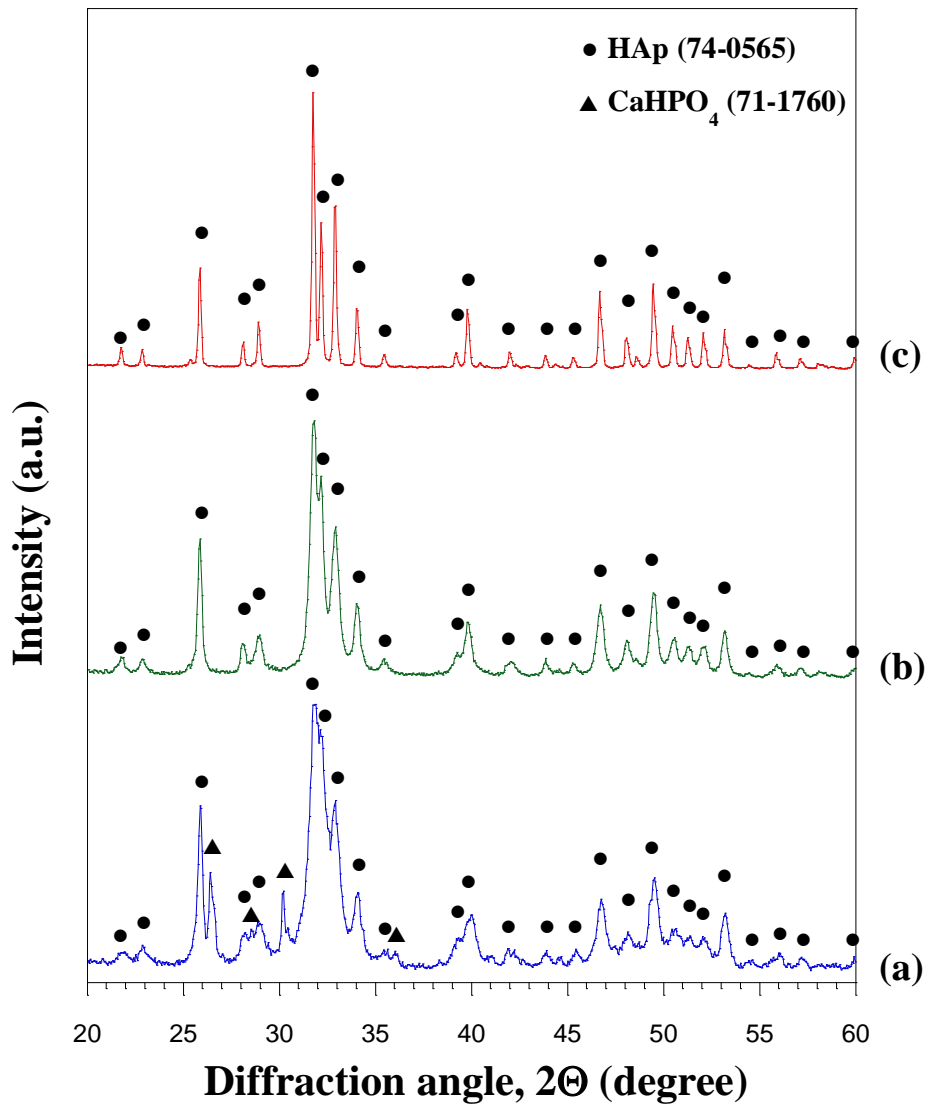
36 **Figure 13.** Mechanical test results performed on **HAp_1**, **HAp_2** and **HAp_3** materials obtained
37 by SPS under optimal sintering conditions: (a) micro-hardness and (b) local elastic
38 modulus.
39
40
41
42
43
44
45
46
47
48
49
50
51
52
53
54
55
56
57
58
59
60
61
62
63
64
65

Figure 1. SEM images at different magnitudes of the initial HAp powders used in the present investigation: (a)-(b) **HAp_1**, (c)-(d) **HAp_2** and (e)-(f) **HAp_3**.



1
2
3
4
5
6
7
8
9
10
11
12
13
14
15
16
17
18
19
20
21
22
23
24
25
26
27
28
29
30
31
32
33
34
35
36
37
38
39
40
41
42
43
44
45
46
47
48
49
50
51
52
53
54
55
56
57
58
59
60
61
62
63
64
65

Figure 2. XRD patterns on the initial HAp powders used in the present work: (a) HAp_1, (b) HAp_2 and (c) HAp_3.



1
2
3
4
5
6
7
8
9
10
11
12
13
14
15
16
17
18
19
20
21
22
23
24
25
26
27
28
29
30
31
32
33
34
35
36
37
38
39
40
41
42
43
44
45
46
47
48
49
50
51
52
53
54
55
56
57
58
59
60
61
62
63
64
65

Figure 3. Effect of the heat treatment in air on the composition of (a) **HAp_1**, (b) **HAp_2** and (c) **HAp_3** powders.

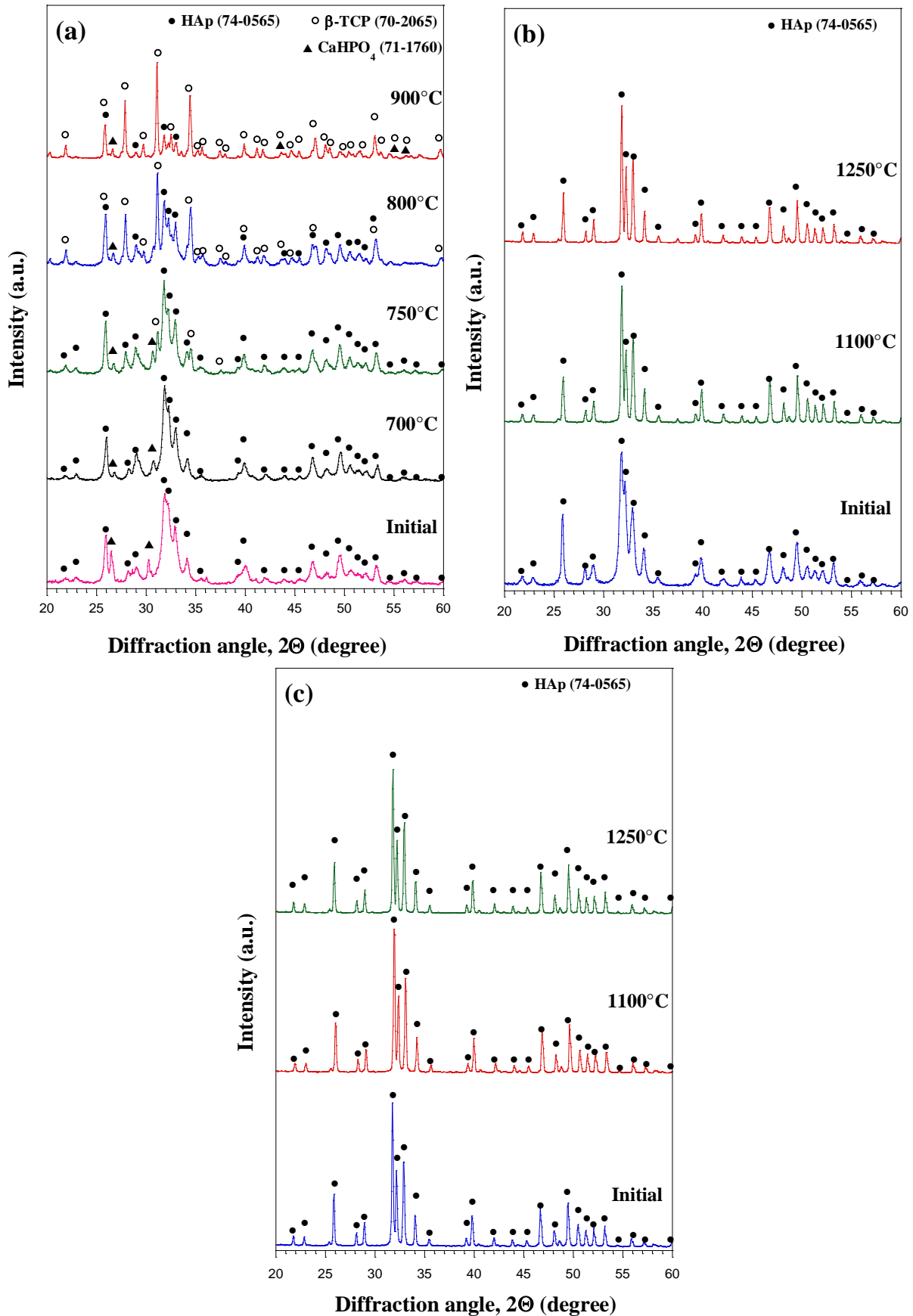
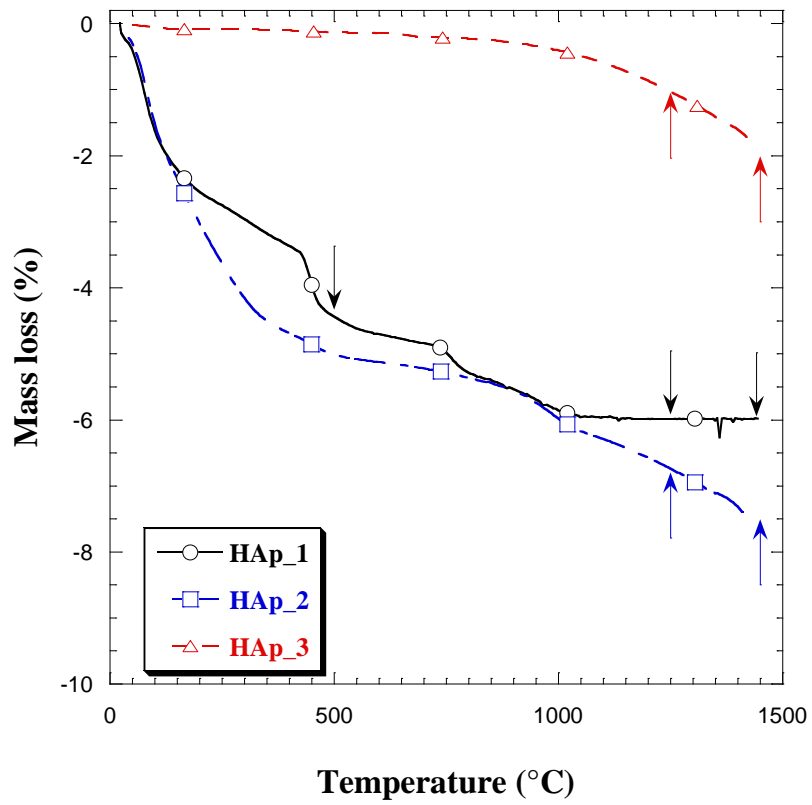


Figure 4. Mass loss of HAp powders during TGA in air.



1
2
3
4
5
6
7
8
9
10
11
12
13
14
15
16
17
18
19
20
21
22
23
24
25
26
27
28
29
30
31
32
33
34
35
36
37
38
39
40
41
42
43
44
45
46
47
48
49
50
51
52
53
54
55
56
57
58
59
60
61
62
63
64
65

Figure 5. Compositional changes of (a) **HAp_1**, (b) **HAp_2** and (c) **HAp_3** powders during TGA (10°C/min) in air (100 ml/min) (cf. **Figure 4**).

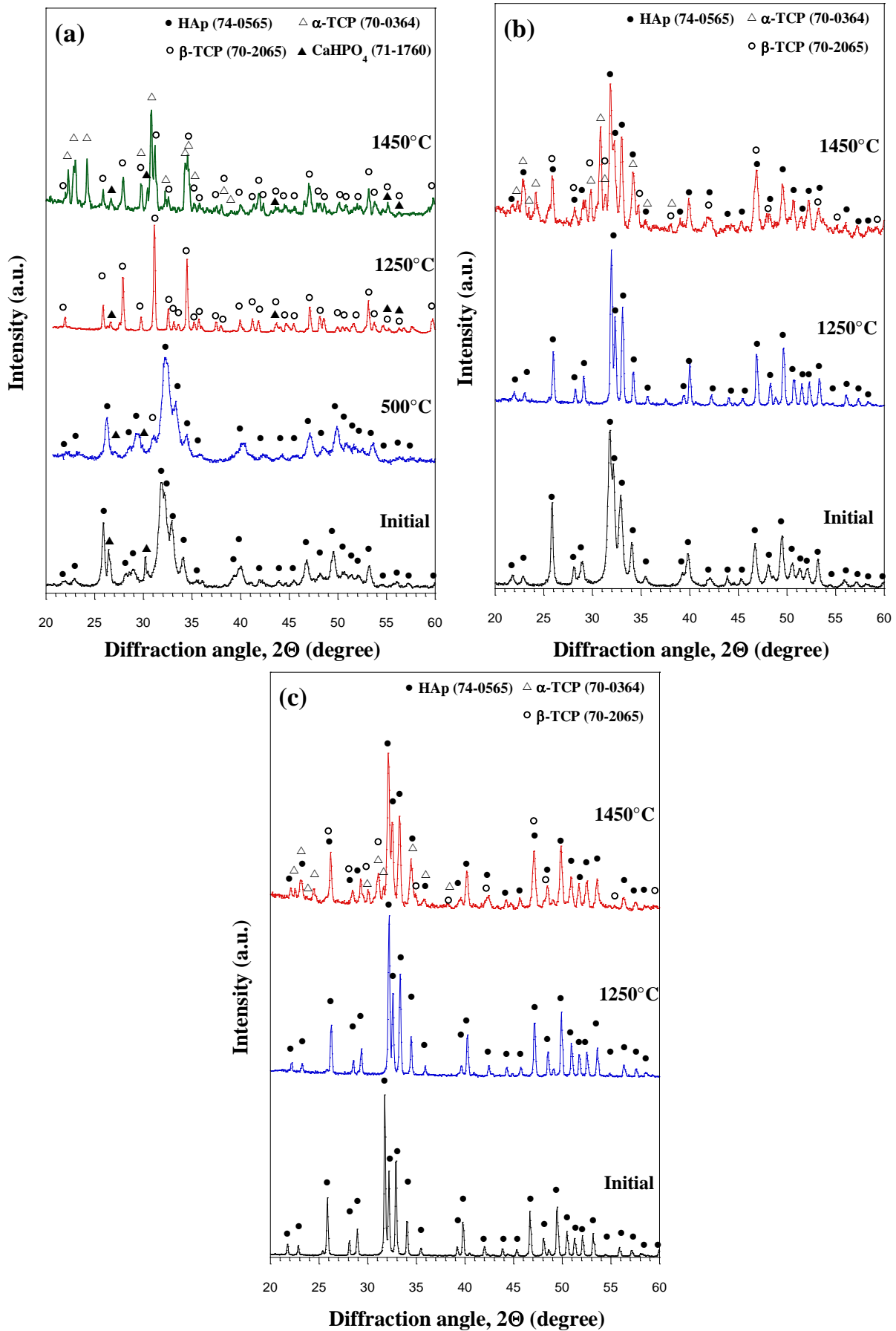
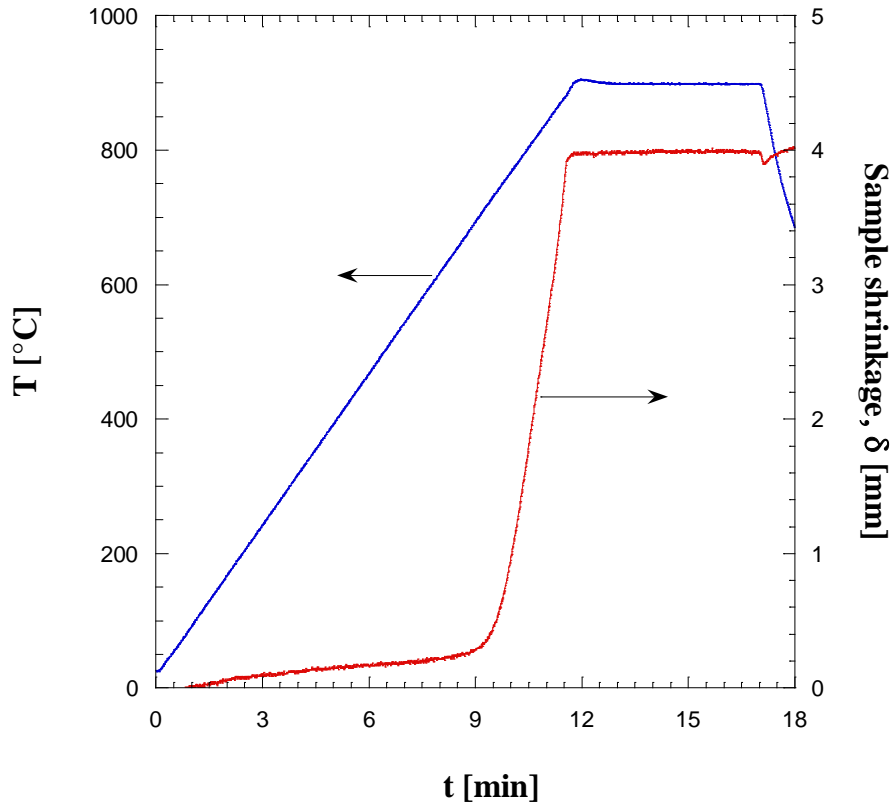
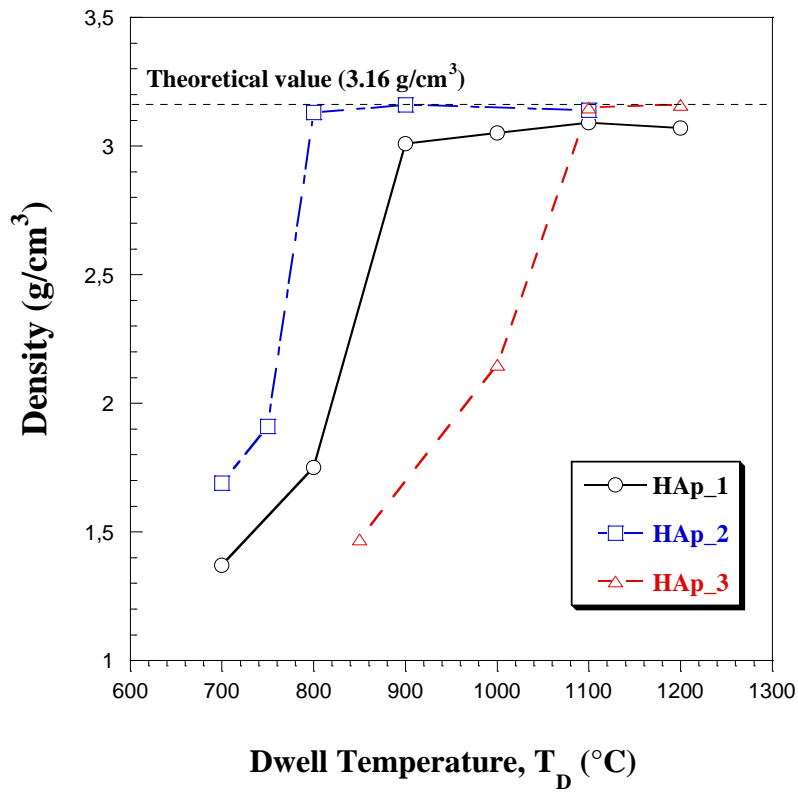


Figure 6. Temperature and sample shrinkage time profiles recorded during consolidation of **HAp_2** powders by SPS (900°C, 75 °C/min, $t_D=5$ min, 30 MPa).



1
2
3
4
5
6
7
8
9
10
11
12
13
14
15
16
17
18
19
20
21
22
23
24
25
26
27
28
29
30
31
32
33
34
35
36
37
38
39
40
41
42
43
44
45
46
47
48
49
50
51
52
53
54
55
56
57
58
59
60
61
62
63
64
65

Figure 7. Influence of the sintering temperature on the density of the HAp products obtained by SPS (75 °C/min, $t_D=5$ min, 30 MPa).



1
2
3
4
5
6
7
8
9
10
11
12
13
14
15
16
17
18
19
20
21
22
23
24
25
26
27
28
29
30
31
32
33
34
35
36
37
38
39
40
41
42
43
44
45
46
47
48
49
50
51
52
53
54
55
56
57
58
59
60
61
62
63
64
65

Figure 8. Comparison of XRD patterns before and after consolidation by SPS (75 °C/min, $t_D=5$ min, 30 MPa) of (a) **HAp_1**, (b) **HAp_2** and (c) **HAp_3** powders.

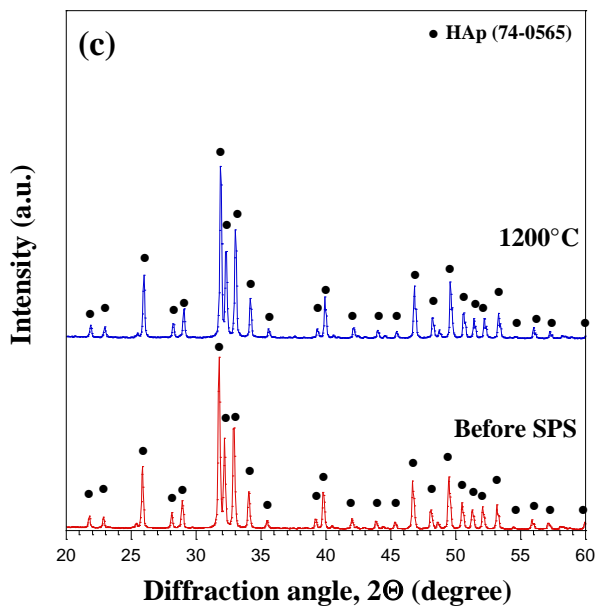
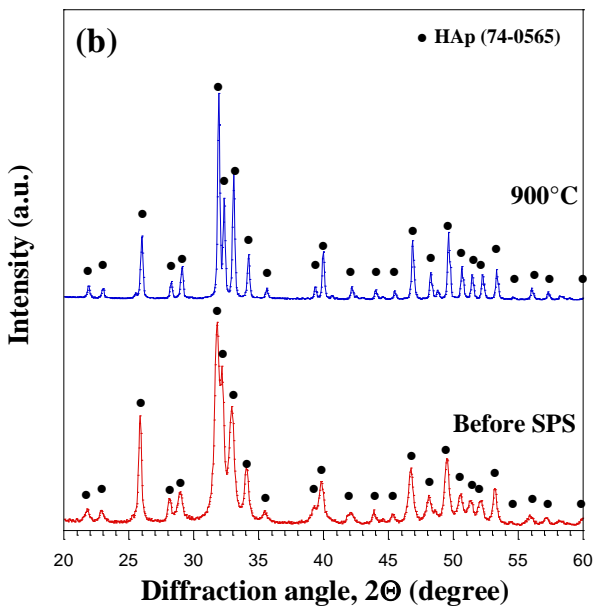
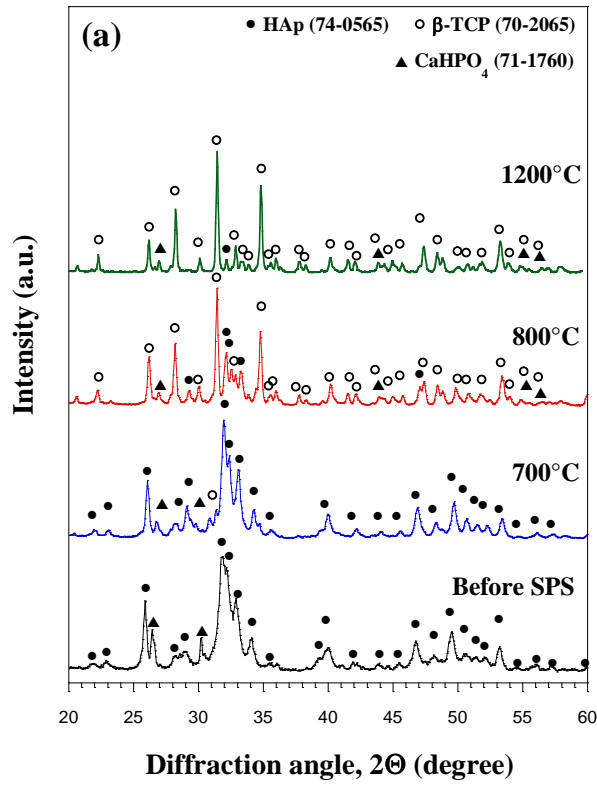
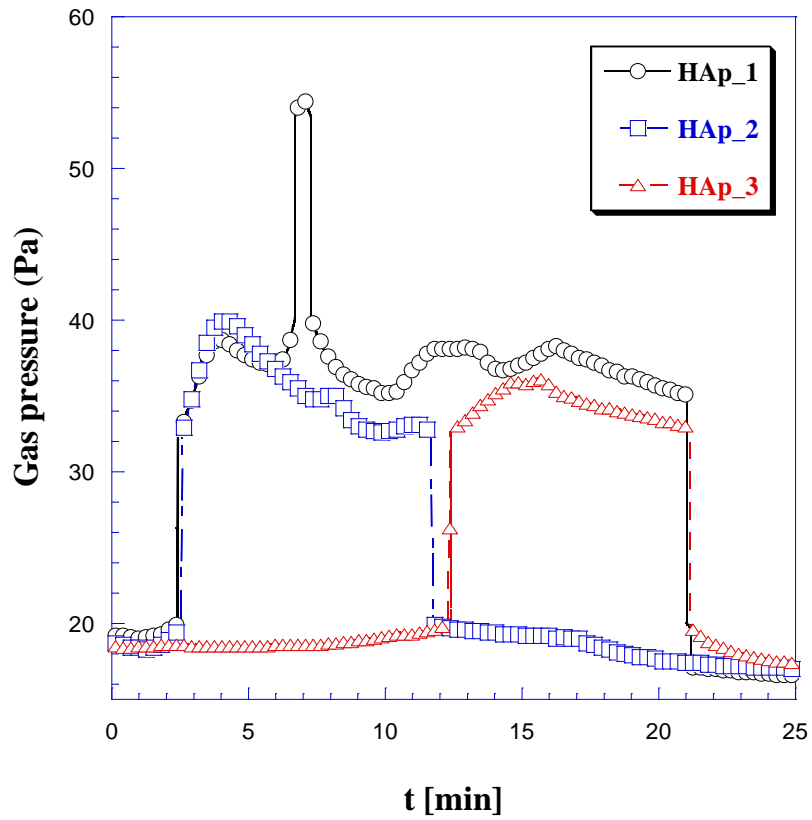


Figure 9. Temporal evolution of gas pressure during the SPS process (75 °C/min, $t_D=5$ min, 30 MPa) of **HAp_1**, **HAp_2** and **HAp_3** powders.



1
2
3
4
5
6
7
8
9
10
11
12
13
14
15
16
17
18
19
20
21
22
23
24
25
26
27
28
29
30
31
32
33
34
35
36
37
38
39
40
41
42
43
44
45
46
47
48
49
50
51
52
53
54
55
56
57
58
59
60
61
62
63
64
65

Figure 10. SEM micrographs (5000x) of chemically etched dense products obtained by SPS under optimal conditions: (a) **HAp_1**, (b) **HAp_2** and (c) **HAp_3**.

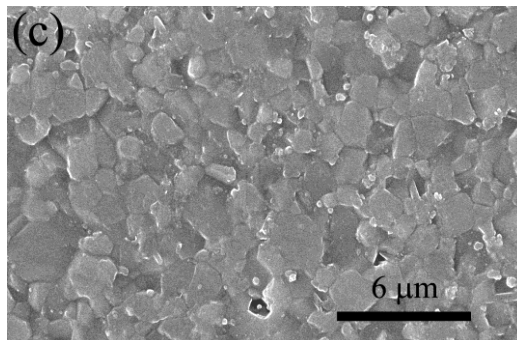
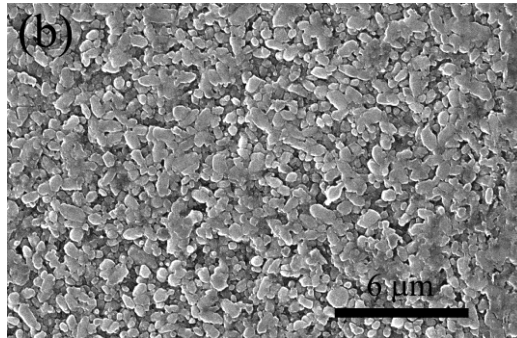
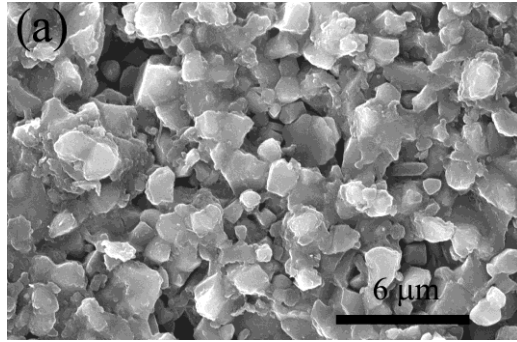
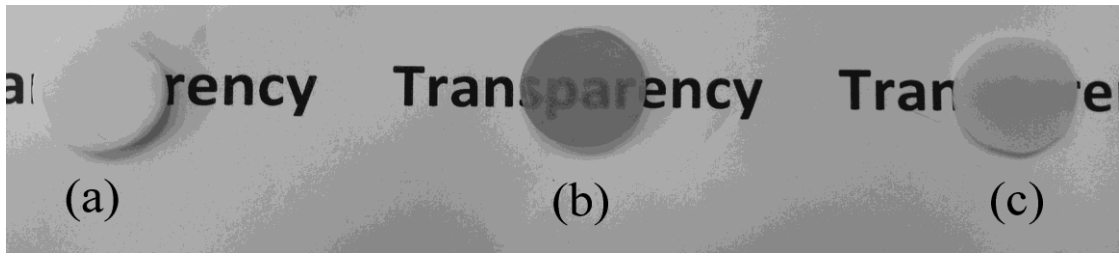


Figure 11. Optical photographs of dense products obtained by SPS under optimal conditions: (a) HAp_1, (b) HAp_2 and (c) HAp_3.



1
2
3
4
5
6
7
8
9
10
11
12
13
14
15
16
17
18
19
20
21
22
23
24
25
26
27
28
29
30
31
32
33
34
35
36
37
38
39
40
41
42
43
44
45
46
47
48
49
50
51
52
53
54
55
56
57
58
59
60
61
62
63
64
65

Figure 12. Residual imprints produced in the cross section of the **HAp_2** samples during indentation tests: (a) 0.5 N and 2.0 N (b) loads.

1
2
3
4
5
6
7
8
9
10
11
12
13
14
15
16
17
18
19
20
21
22
23
24
25
26
27
28
29
30
31
32
33
34
35
36
37
38
39
40
41
42
43
44
45
46
47
48
49
50
51
52
53
54
55
56
57
58
59
60
61
62
63
64
65

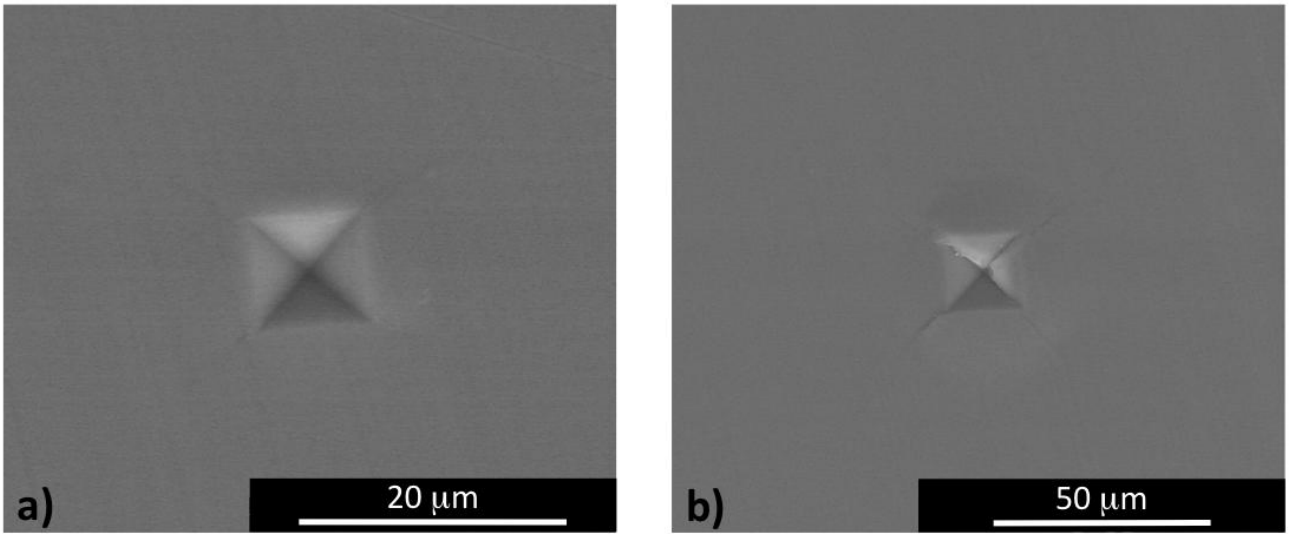
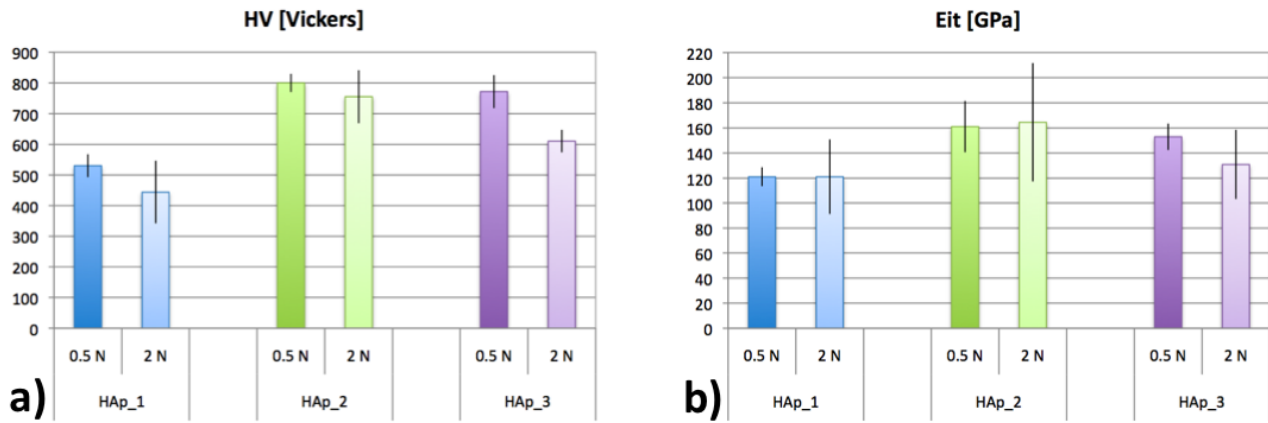


Figure 13. Mechanical test results performed on **HAp_1**, **HAp_2** and **HAp_3** materials obtained by SPS under optimal sintering conditions: (a) micro-hardness and (b) local elastic modulus.



1
2
3
4
5
6
7
8
9
10
11
12
13
14
15
16
17
18
19
20
21
22
23
24
25
26
27
28
29
30
31
32
33
34
35
36
37
38
39
40
41
42
43
44
45
46
47
48
49
50
51
52
53
54
55
56
57
58
59
60
61
62
63
64
65

1 **Consolidation of different Hydroxyapatite powders by SPS: optimization of the**
2
3
4 **sintering conditions and characterization of the obtained bulk products**
5
6
7
8
9

10
11
12
13 A. Cuccu¹, S. Montinaro¹, R. Orrù^{1,*}, G. Cao¹, D. Bellucci², A. Sola², V. Cannillo²
14
15
16

17
18 ¹*Dipartimento di Ingegneria Meccanica, Chimica e dei Materiali, Unità di Ricerca del*
19
20 *Consorzio Interuniversitario Nazionale per la Scienza e Tecnologia dei Materiali*
21
22 *(INSTM) - Università degli Studi di Cagliari, via Marengo 2, 09123 Cagliari, Italy*
23
24

25 ²*Dipartimento di Ingegneria “Enzo Ferrari”, Università degli Studi di Modena e*
26
27 *Reggio Emilia, Via Vignolese 905, 41125 Modena, Italy*
28
29
30

31
32
33
34
35 * Author to whom correspondence should be addressed:
36

37 R. Orrù (E-mail: roberto.orrù@dimcm.unica.it; Ph.: +39-070-6755076; Fax: +39-070-
38
39 6755057), *Università degli Studi di Cagliari, via Marengo 2, 09123 Cagliari, Italy*
40
41
42
43
44
45

46
47 Revised Version
48

49 **August 2014**
50
51
52
53
54
55
56
57
58
59
60
61
62
63
64
65

1 **Abstract**
2

3 The difference in purity, particle size, microstructure, and thermo-chemical
4 stability of three commercially available hydroxyapatite powders are found to play an
5 important role during their consolidation using Spark Plasma Sintering (SPS) as well as
6 strongly affect the characteristics of the resulting sintered bodies. A fully dense material
7 without secondary phases was obtained by SPS at 900°C, when using the relatively
8 small sized, with refined grains and high purity powders. The sintered product,
9 consisting of sub-micrometer sized hydroxyapatite grains, displayed optical
10 transparency and good mechanical properties.
11
12

13 In contrast, the higher temperature levels (up to 1200 °C) needed to sinter
14 powders with larger particles, or finer ones which contain additional phases, lead to
15 products with coarser microstructures and/or significant amount of β -TCP as a result of
16 HAp decomposition. Optical characteristics, hardness and elastic modulus of the
17 resulting sintered samples are correspondingly worsened.
18
19
20
21
22

23 *Keywords:* Hydroxyapatite; Tri-Calcium Phosphate (TCP), Spark Plasma Sintering;
24
25
26
27
28
29
30
31
32
33
34
35
36
37
38
39
40
41
42 Mechanical properties
43
44
45
46
47
48
49
50
51
52
53
54
55
56
57
58
59
60
61
62
63
64
65

1. Introduction

Since hydroxyapatite ($\text{Ca}_{10}(\text{PO}_4)_6(\text{OH})_2$), often referred to as HAp or HA, represents the main inorganic component of hard human tissues (bones and teeth), it is not surprising that it is regarded as one of the most investigated ceramics for biomedical application in either bulk form or as coating [1-3].

Due to its importance, a large number of research studies addressed to the fabrication of bulk HAp products using pressureless and pressure-assisted sintering methods, mainly conventional Hot Pressing (HP) or innovative Spark Plasma Sintering (SPS) techniques, have been conducted so far [2].

It is well known that one of the main concerns accompanying heat processing of HAp is related to its thermochemical instability [4]. Indeed, HAp decomposition takes place when relatively high temperature conditions are encountered during powder consolidation. Correspondingly, negative effects on mechanical and biological characteristics of the resulting materials are often produced.

In this context, the SPS technology offers a suitable method for obtaining bulk ceramic products under relatively milder sintering conditions [5]. Indeed, the electric pulsed current flowing directly through the die containing the non-conductive HAp powders permits sample heating at higher rates and in shorter processing times with respect to conventional HP, where external elements are employed as heating source.

Along these lines, several studies have been conducted in the literature in the last decade for the fabrication of dense HAp ceramics by SPS [6-19]. Most of them take advantage of the SPS technology for the consolidation of previously synthesized lab-made [6,8-11,13-15,17,19] or commercial [7,10,16,18-19] HAp powders. Alternatively,

1 one attempt to synthesize and simultaneously densify the HAp by reactive SPS was
2
3 carried out starting from $\text{CaHPO}_4 \cdot 2\text{H}_2\text{O}$ and $\text{Ca}(\text{OH})_2$ as reaction promoters [12].
4
5

6 As a consequence of the different starting materials, the operating conditions
7
8 (i.e. holding temperature, heating rate, applied pressure and dwell time) adopted in these
9
10 studies to obtain nearly full dense HAp-based bodies vary in a quite wide range, i.e.
11
12 700-1200°C. However, the potential benefits deriving from the use of SPS are
13
14 confirmed. In this regard, it is clear that the characteristics of the initial powders deeply
15
16 affect the final composition as well as the resulting mechanical and biological properties
17
18 of the sintered material. Indeed, the decomposition of HAp to produce Tri-Calcium
19
20 Phosphate (TCP) [8,11,15] could not be associated only to the more drastic SPS
21
22 conditions correspondingly adopted. For instance, no additional phases other than HAp
23
24 were found in the 99.7% dense material fabricated in 10 min by SPS at 1200°C [9]. On
25
26 the other hand, the presence of β -TCP was evidenced by Lee et al. [11] in the 96.4%
27
28 dense material obtained when the sintering process was conducted at 1000°C for 2 min.
29
30 The use of different SPS apparatuses and sample configurations might also play a role
31
32 in this regard.
33
34
35
36
37
38
39

40 In order to systematically investigate the influence of the characteristics of the
41
42 initial powders on the final composition as well as the resulting mechanical properties,
43
44 in the present work bulk HAp ceramics are produced by SPS using three different
45
46 commercially available powders. The starting materials are first characterized by laser
47
48 scattering analysis, X-ray diffraction (XRD), SEM, heat treatments in air and
49
50 thermogravimetric analysis in order to highlight their main differences (purity, particle
51
52 and crystallite size, thermochemical stability, etc.). Each HAp powder is then
53
54 consolidated by SPS. In particular, a systematic investigation is performed to identify
55
56
57
58
59
60
61
62
63
64
65

1 the optimal sintering temperatures to obtain fully dense products, while keeping all the
2
3 other parameters unchanged (SPS equipment, applied pressure, heating rate, holding
4
5 time, sample configuration). The resulting optimal samples are compared from the
6
7
8 compositional, microstructural and mechanical point of view.
9

10
11
12
13
14
15
16
17
18
19
20
21
22
23
24
25
26
27
28
29
30
31
32
33
34
35
36
37
38
39
40
41
42
43
44
45
46
47
48
49
50
51
52
53
54
55
56
57
58
59
60
61
62
63
64
65

2. Experimental materials and methods

The main characteristics, as provided by the vendors, of the three different commercial powders investigated in this work for the fabrication of dense HAp products are reported in **Table 1**. A more detailed particle size analysis was carried out in the present study taking advantage of a laser light scattering analyser (CILAS 1180, France). The starting powders were also examined by XRD using a Philips PW 1830 X-rays diffractometer equipped with a Ni filtered Cu K α radiation ($\lambda=1.5405$ Å). The powders' morphology was investigated by scanning electron microscopy (SEM, mod. S4000, Hitachi, Japan).

The thermal stability of the HAp powders was studied by heat treating the raw materials in air environment at different temperatures, in the range of 700-1250°C, using a laboratory furnace (Nabertherm, mod. N60/ER, Germany). In addition, a thermogravimetric analysis (TGA) under non-isothermal conditions was carried out by slowly heating (10°C/min) the initial powders from room temperature to 1450°C using a NETZSCH STA 409PC Simultaneous DTA-TGA Instrument in presence of 100 mL/min air flow.

The HAp powders were sintered in the form of cylindrical disks (about 15 mm diameter, 3 mm thickness) by Spark Plasma Sintering (SPS 515S model, Sumitomo Coal Mining Co Ltd) under vacuum conditions (20 Pa). This apparatus is based on the combination of a uniaxial press (50 kN) with a DC pulsed current generator (10 V, 1500 A, 300 Hz), thus simultaneously providing a pulsed electric current through the sample (when electrically conductive) and the graphite container, along with a mechanical pressure through the punches. The pulse cycle was set to 12 ms on and 2 ms off, being the characteristic time of single pulse equal to about 3.3 ms. Both the die and the

1 plungers were made of AT101 graphite (Atal s.r.l., Italy). The powders to be sintered
2
3 (about 1.6 g) were poured inside a cylindrical graphite die with outside diameter of 35
4
5 mm, inside diameter of 15 mm, and 30 mm high. To protect the die/plungers and make
6
7 sample release easier after sintering, the compact was lined with a graphite foil (0.13
8
9 mm thick, Alfa Aesar Karlsruhe, Germany). In addition, the die was surrounded by a
10
11 layer of graphite felt (3 mm thick, Atal s.r.l., Italy) for thermal insulation purpose.
12
13
14

15
16 The most important SPS parameters, i.e. temperature, current, voltage between
17
18 the machine electrodes, mechanical load and vertical sample displacement, were
19
20 recorded in real time. The displacement output provides an indication of the evolution
21
22 of the powders' densification during SPS. However, the thermal expansion of sample,
23
24 electrodes, graphite blocks, spacers and plungers is also responsible for the measured
25
26 value. All these contributions, but that of the sample, can be separately accounted for by
27
28 following a specific procedure [20], thus obtaining the sample shrinkage (δ), which will
29
30 be considered in what follows. In any case, the final consolidation level was determined
31
32 by measuring the density of the samples obtained at the end of the SPS process. After
33
34 sintering, the electric current was turned off, the mechanical load released, the sample
35
36 allowed to cool to room temperature and then removed from the die. For the sake of
37
38 reproducibility, each experiment was repeated at least twice.
39
40
41
42
43
44

45 SPS experiments were conducted under temperature controlled mode using a K-
46
47 type thermocouple (Omega Engineering Inc., USA) inserted inside a small hole drilled
48
49 near the center of the external surface of the graphite die. Temperature levels were also
50
51 measured by means of an infrared pyrometer (CHINO, mod. IR-AHS2, Japan) focused
52
53 on the lateral surface of the graphite mould.
54
55
56
57
58
59
60
61
62
63
64
65

1 The effect of the dwell temperature, T_D , on the product characteristics was
2
3 investigated by performing all SPS experiments at constant values of the holding time
4
5 ($t_D=5$ min), the mechanical pressure ($P=30$ MPa), and the heating rate ($75^\circ\text{C}/\text{min}$), to
6
7 achieve the desired value from the room temperature.
8
9

10 Relative densities were determined by the Archimedes' method after accurately
11
12 polishing SPSed products and considering $3.16\text{ g}/\text{cm}^3$ as theoretical value.
13
14

15 The microstructure of the optimal SPSed products was examined by SEM. To this
16
17 aim, the sintered specimens were first mirror polished and then chemically etched for 10
18
19 s using a 3 vol.% HNO_3 solution.
20
21

22 The selected samples were also investigated from a mechanical point of view. A
23
24 depth-sensing indentation technique was applied to determine the local elastic modulus
25
26 and Vickers micro-hardness. With this aim, the samples were cut, mounted in resin and
27
28 polished according to a standard metallographic procedure. The indentations were
29
30 performed using an OpenPlatform instrument (CSM Instruments, Peseux, Switzerland),
31
32 equipped with a Vickers indenter tip. For each sample, two different loading conditions
33
34 were considered:
35
36

37 - low load: maximum applied load: 0.50 N; loading/unloading rate: 0.75 N/min;
38
39 loading time: 15 s;
40
41

42 - high load: maximum applied load: 2.00 N; loading/unloading rate: 3.00 N/min;
43
44 loading time: 15 s.
45
46

47 For statistical purposes, 30 indentations were performed for each sample and for each
48
49 loading condition. For each indentation, the load-penetration depth curve was
50
51 automatically acquired and then analyzed according to the Oliver and Pharr method to
52
53 evaluate the local elastic properties [21].
54
55
56
57
58
59
60
61
62
63
64
65

1 **3. Results and discussion**

2
3 **3.1 Characterization of initial powders**

4
5
6 The results related to the granulometry of the three different types of powders
7
8 measured by laser light scattering analysis are summarized in **Table 2**. While **HAp_1**
9
10 and **HAp_2** systems display similar fine particles, **HAp_3** powders are relatively
11
12 coarser. This feature is clearly confirmed when examining the corresponding SEM
13
14 micrographs (**Figure 1**). Specifically, both **HAp_1** and **HAp_2** materials generally
15
16 consist of micrometer-sized aggregates made of sub-micrometer grains. In contrast, the
17
18 **HAp_3** product exhibits coarser particles, up to 100 μm sized, characterized by a
19
20 sponge like structure with pores down to 100 nm (**Figure 1(f)**).
21
22
23
24

25 The comparison of the corresponding XRD patterns is shown in **Figure 2**. On the
26
27 basis of this analysis it is possible to state that HAp is the only phase present in **HAp_2**
28
29 and **HAp_3**, while a non-negligible amount of CaHPO_4 was detected in **HAp_1**
30
31 powders. In addition, the **HAp_1** and **HAp_2** systems displayed relatively broad
32
33 diffraction peaks, to indicate their finer microstructure, in contrast to the narrow peaks
34
35 observed when considering the **HAp_3** material.
36
37
38
39

40 The thermal stability of the starting powders was first evaluated by heat-treating
41
42 the different raw materials in a furnace under air environment. The XRD spectra of the
43
44 heat-treated powders are reported in **Figures 3(a)-(c)**.
45
46

47 No additional phases were detected by XRD when the **HAp_1** system was heat-
48
49 treated at temperatures equal or lower than 700°C. On the other hand, as the
50
51 temperature was raised to 750°C, the β -TCP phase (rhombohedral lattice) appeared in
52
53 the XRD pattern of the end product. In addition, as higher thermal levels were achieved,
54
55 the decomposition of HAp was found to increase progressively. Specifically, β -TCP
56
57
58
59
60
61
62
63
64
65

1 becomes the major crystalline constituent in powders heat treated at 900°C, while only
2
3
4 minor amounts of HAp and CaHPO₄ are present.

5
6 On the other hand, as evidenced in **Figures 3(b)** and **3(c)**, no secondary species
7
8 are found in XRD patterns of **HAp_2** and **HAp_3** powders heat-treated up to 1250°C.
9
10 The most significant change, particularly for **HAp_2**, is represented by a certain peak
11
12 narrowing, with respect to the original material, thus indicating that grain growth is
13
14 induced by the heat treatment.
15
16

17
18 In order to overcome the temperature limitation (1300°C) of the furnace utilized
19
20 in the previous heat-treatment as well as to obtain further information regarding the
21
22 chemico-physical stability of the powders under consideration, the latter ones have been
23
24 also characterized by TGA up to 1450°C. The corresponding mass losses as a function
25
26 of the temperature are plotted in **Figure 4** for the three systems. It is possible to observe
27
28 that only for temperatures above 1000°C the **HAp_3** material significantly changes its
29
30 mass. In contrast, the curves corresponding to the other two products markedly decrease
31
32 just after the TGA test starts. Moreover, the weight losses resulting at the end of the
33
34 experiment for **HAp_1** and **HAp_2** are 3-4 times higher than the value obtained when
35
36 processing the **HAp_3** material.
37
38
39
40
41

42
43 The mass loss profiles described above can be associated to the compositional
44
45 changes taking place in the powders as the temperature increases during the TGA test.
46
47 This information was obtained by interrupting the experiments at different time
48
49 intervals corresponding to the arrows indicated in **Figure 4** and analyzing by XRD the
50
51 related products. The obtained results are shown in **Figure 5(a)-5(c)**. As far as the
52
53 **HAp_1** is concerned, it is seen that the formation of β-TCP is evidenced at relatively
54
55 low temperature (500°C), i.e. immediately after the sudden slope change manifested by
56
57
58
59
60
61
62
63
64
65

1 the mass loss curve (**Figure 4**). Nevertheless, the corresponding sample weight loss
2
3 could be mostly ascribed to the occurrence of dehydroxylation phenomena.
4

5
6 The XRD analysis performed when the TGA test for the **HAp_1** system was
7
8 conducted at 1250°C indicated that a complete decomposition of HAp to β -TCP
9
10 occurred. Minor amounts of CaHPO_4 , originally present in the raw material, were also
11
12 found at this stage. Furthermore, as the thermal analysis was prolonged to 1450°C, it is
13
14 possible to observe a significant conversion of TCP from the β to the α (monoclinic)
15
16 form, which represents the thermodynamically stable phase at high temperatures. This
17
18 outcome is consistent with the fact that the transformation of β -TCP into the α - form is
19
20 commonly reported to occur at temperatures above 1120-1170°C [2].
21
22
23
24

25 In contrast, as evidenced in **Figure 4(b)**, no additional peaks are detected in XRD
26
27 patterns of the **HAp_2** product subjected to TGA at 1250°C. This feature clearly
28
29 confirms its higher thermal stability with respect to the **HAp_1** system. Therefore, the
30
31 significant weight loss (about 7%) observed at 1250°C for this system (**Figure 4**) can be
32
33 only associated to the dehydroxylation of HAp. Nevertheless, a completely different
34
35 situation is encountered when the temperature is raised to 1450°C. Indeed, a
36
37 considerable amount of TCP, particularly in its α - form, is present in the end product
38
39 along with residual HAp.
40
41
42
43
44

45 A behavior qualitatively similar to that described for **HAp_2** was also displayed
46
47 by the **HAp_3** material, which also exhibited a relatively high thermal stability.
48
49 Specifically, as shown in **Figure 5(c)**, HAp was the only phase found by XRD in
50
51 powders subjected to TGA at 1250°C. In addition, it should be noted that the amount of
52
53 α - and β -TCP formed when the temperature was increased to 1450°C is even lower with
54
55 respect to that found in the **HAp_2** material.
56
57
58
59
60
61
62
63
64
65

1 In conclusion, on the basis of the results obtained when heat treating in air the
2 three HAp systems, **HAp_1** powders is found to display a marked thermal instability as
3 HAp decomposes at rather low temperatures. In contrast, when the **HAp_2** and **HAp_3**
4 HAp decomposes at rather low temperatures. In contrast, when the **HAp_2** and **HAp_3**
5 powders are heat-treated in air flow, the transformation of HAp takes place only at
6 temperatures above 1250°C to produce TCP, particularly in its α - configuration.
7 Furthermore, the significant weight loss displayed by **HAp_1** and **HAp_2** in
8 comparison to **HAp_3** could be likely associated to their relatively larger surface area
9 due to the corresponding finer particles size, so that the occurrence of dehydroxylation
10 phenomena is facilitated.
11
12
13
14
15
16
17
18
19
20
21

22 As far as the different thermal stability exhibited by the three HAp powders under
23 examination is concerned, it should be noted that the minimum temperature to which
24 calcium phosphate apatites decompose is well known to depend on several factors such
25 as powders purity, particles size and shape, Ca/P molar ratio, as well as the
26 environmental conditions under which the heat treatment is carried out [4; 22-24]. Thus,
27 the decomposition of HAp to β -TCP taking place at relatively low temperature for the
28 case of HAp_1 system can be readily ascribed to the presence of secondary phases
29 (CaHPO_4) in the corresponding starting powders. In addition, the transformation
30 temperature of about 750°C found in this case during heat treatment experiments in air
31 furnace (cf. **Figure 3a**) is in agreement with **Graeve et al. [24]** findings. Specifically, in
32 the latter study, no indication of compositional changes was evidenced by XRD after
33 powder calcination at 600°C, whereas β -TCP was clearly detected at 800°C. A
34 dissociation temperature of HAp to β -TCP of about 700°C was also reported in the
35 literature relatively to heat-treated calcium phosphate apatites with $1.5 < \text{Ca/P} < 1.667$
36 [23]. The fact that during the TGA experiments conducted in the present study, β -TCP
37
38
39
40
41
42
43
44
45
46
47
48
49
50
51
52
53
54
55
56
57
58
59
60
61
62
63
64
65

1 was already detected at 500°C (cf. **Figure 5a**) might be likely due to the air flow
2
3 conditions adopted during this analysis which, apparently, are able to anticipate HAp
4
5 decomposition.
6
7

8 Differently from the HAp₁ system, the characteristics of HAp₂ and HAp₃
9
10 powders, particularly their relatively higher purity, make them more thermally stable. In
11
12 this regard, it should be noted that the temperature levels (above 1250°C) at which HAp
13
14 was found to decompose to α -TCP (cf. **Figures 3** and **5**) are also well in agreement with
15
16 the interval of 1350-1400°C reported in the literature on this subject [**4**; **22**].
17
18
19
20
21
22

23 **3.2 Powders consolidation by SPS**

24
25 Typical outputs of sample shrinkage (δ) and temperature obtained during the
26
27 densification process by SPS of HAp powders are reported in **Figure 6** for the case of
28
29 the **HAp₂** system. Specifically, these data refer to the conditions of $T_D=900$ °C, 75
30
31 °C/min heating rate, $t_D=5$ min, and $P=30$ MPa. Only minor changes in the sample
32
33 shrinkage are observed during the first 9 min of the SPS process, i.e. for temperatures
34
35 below 700°C. On the other hand, as the temperature is raised above that level, the slope
36
37 of the sintering curve rapidly increases approximately at a constant rate to reach a
38
39 sample shrinkage of about 4 mm when the dwell temperature is achieved. Afterwards,
40
41 the δ parameter modestly varies up to the end of the SPS experiment. Analogous
42
43 qualitative comments can be made when examining the sintering behavior of the other
44
45 systems and/or consolidation conditions investigated.
46
47
48
49
50
51

52 The effect of the dwell temperature on SPSed product density is shown in
53
54 **Figure 7** for the different HAp materials taken into account in the present work. All the
55
56 plotted data refer to sintering experiments conducted at 30 MPa, $t_D=5$ min and 75
57
58
59
60
61
62
63
64
65

1 °C/min heating rate. As expected, the sample densification is improved as the sintering
2
3 temperature is increased, although the three processed powders displayed a quite
4
5 different behavior. Indeed, while the **HAp_2** material achieved a high consolidation
6
7 level at 800°C, the density values obtained by the other two materials, when processed
8
9 under the same conditions, are still extremely low. In particular, the temperature
10
11 condition required to produce fully dense **HAp_2** samples is 900°C, whereas the
12
13 optimal temperature to achieve the same goal when starting from **HAp_3** powders is
14
15 1200°C. A peculiar behavior is observed when optimizing the sintering process for the
16
17 **HAp_1** system. Specifically, a significant sample densification was evidenced in the
18
19 range of 800-900°C, while a further temperature increase was accompanied only by a
20
21 slight change in product density and the theoretical density value of 3.16 g/cm³ was not
22
23 achieved even at 1200°C.
24
25
26
27
28
29

30 The comparison of the XRD patterns of the original powders with the
31
32 corresponding SPS products obtained under optimal sintering conditions is shown in
33
34 **Figures 8(a)-8(c)** for the three systems.
35
36

37 As far as the **HAp_1** system is concerned, the first evidence of TCP formation is
38
39 observed at 700°C, i.e. when the sample is less than 50% dense (**Figure 7**). Moreover,
40
41 an increase of the temperature level up to 800°C is accompanied by a marked
42
43 decomposition of HAp to β -TCP, which becomes the major phase in the SPS product.
44
45 The amount of HAp tends to disappear when the sintering temperature is increased to
46
47 1200°C, and the corresponding material consists mainly of β -TCP. Minor amounts of
48
49 CaHPO₄ are still detected, as in the related starting powders. Thus, the fact that the
50
51 density of the SPSed product for the **HAp_1** system does not reach the theoretical value
52
53
54
55
56
57
58
59
60
61
62
63
64
65

1 of pure HAp (**Figure 7**) can be readily ascribed to the compositional changes of the
2
3 processing sample during SPS.
4

5
6 In contrast to the behavior described above for the **HAp_1** material and in
7
8 agreement with the results obtained with the heat-treatment of raw powders, the other
9
10 two systems exhibit a higher thermochemical stability during SPS. Indeed, regardless
11
12 the different dwell temperatures required to obtain fully dense materials, **Figures 8(b)**
13
14 and **8(c)** clearly indicate that no secondary phases are found by XRD in the fully dense
15
16 **HAp_2** and **HAp_3** samples, respectively.
17
18

19
20 Interesting information in this regard can be also obtained when examining the
21
22 gas pressure evolution inside the SPS chamber during the consolidation process. It
23
24 should be noted that a vacuum pump operates continuously to maintain the pressure
25
26 level in the sintering vessel at about 20 Pa. As shown in **Figure 9**, where the recorded
27
28 pressure data are plotted as a function of the SPS time, a completely different behavior
29
30 is exhibited by the three systems undergoing sintering. As far as the **HAp_1** and **HAp_2**
31
32 powders are concerned, it is seen that after about 2.5 min, i.e. when the measured
33
34 temperature was just above 200°C, the pressure value increased rapidly from the initial
35
36 value to approximately 40 Pa. This fact can be associated to the beginning of
37
38 dehydroxylation phenomena for both systems. However, for the case of **HAp_1**, an
39
40 additional sudden increase in the pressure level was observed at about 7 min. This event
41
42 began when the measured temperature was of about 500°C and can be ascribed to the
43
44 initial transformation $\text{HAp} \rightarrow \beta\text{-TCP}$. Indeed, the XRD analysis relative to TGA samples
45
46 (**Figure 5(a)**) evidenced the incipient presence of $\beta\text{-TCP}$ at 500°C. In addition, it is
47
48 important to note that when considering the **HAp_1** material, a relatively high pressure
49
50 level is observed during the entire duration of the consolidation process, thus providing
51
52
53
54
55
56
57
58
59
60
61
62
63
64
65

1 an indication of the progress of the hydroxyapatite decomposition. This fact is
2 confirmed by the XRD analysis of the corresponding specimen (**Figure 8(a)**). On the
3
4 other hand, during the sintering of **HAp_2** powders, the gas pressure first increases, as
5
6 mentioned above, then slightly decreases and finally drops down to the initial level at
7
8 about 12 min. On the basis of the XRD analysis results discussed previously, it is
9
10 possible to state that the change in gas pressure for the **HAp_2** system can be only due
11
12 to water losses. In addition, the fact that no gas expulsion from the sample is evidenced
13
14 during the isothermal stage at 900°C, allows us to conclude that dehydroxylation
15
16 phenomena correspondingly cease to occur.
17
18
19
20
21

22
23 In contrast to the previous finding, when the **HAp_3** powders are taken into
24
25 account, the sudden pressure increase is observed only for a relatively longer sintering
26
27 time, i.e. at about 12.5 min, when temperature levels above 1000°C are achieved. This
28
29 outcome, which is consistent with the results obtained by TGA (**Figure 4**) as well as
30
31 with the corresponding sample composition, still confirms its high thermochemical
32
33 stability with respect to **HAp_1** and **HAp_2**.
34
35
36

37
38 **Figures 10(a)-10(c)** show three SEM micrographs of the sintered products
39
40 obtained by SPS under optimal conditions, after being etched with a HNO₃ solution, as
41
42 described in the Experimental section. First of all, it is seen that the **HAp_1** system,
43
44 mostly consisting of 1-3 μm sized grains of β-TCP (**Figure 10(a)**), appears to be more
45
46 sensitive, as compared to the other competitive material, to the chemical etching
47
48 treatment. This feature provides an indication of the fact that HAp decomposition leads
49
50 to a material which is relatively less resistant to aggressive environments. In addition, it
51
52 is clear that a relatively finer microstructure, with respect to the other systems, is
53
54 obtained in **HAp_2** products, as demonstrated by the corresponding sub-micrometer
55
56
57
58
59
60
61
62
63
64
65

1 sized hydroxyapatite grains evidenced by the SEM micrograph shown in **Figure 10(b)**.
2
3 In contrast, the sintered **HAp_3** specimen is made of relatively coarser HA grains, up to
4
5 1-3 μm in size. Such differences in the microstructure of the bulk products can be
6
7 readily ascribed to the characteristics of the original powders as well as to the relatively
8
9 milder sintering conditions required when processing **HAp_2** powders (**Figure 7**).
10
11

12
13 Three optical photos corresponding to optimal dense samples, about 2.4 mm
14
15 thick, of the investigated HAp systems are reported in **Figures 11(a)-11(c)**. The product
16
17 which displays a relatively higher transparency is **HAp_2** followed by **HAp_3**, whereas
18
19 **HAp_1** appears to be the most opaque material. Such finding is consistent with the
20
21 results described above. Indeed, the **HAp_2** system is obtained from the relatively more
22
23 refined starting powders and no HAp decomposition was detected during the
24
25 consolidation process. On the other hand, the lack of transparency in the SPSed sample
26
27 obtained using **HAp_1** powders could be likely associated to the significant chemical
28
29 transformations taking place during SPS (**Figure 8(a)**). Finally, although no secondary
30
31 phases have been detected in the sintered **HAp_3** specimen, its relatively coarse
32
33 microstructure could be responsible for the corresponding lower transparency.
34
35
36
37
38
39
40
41

42 **3.3 Mechanical characterization**

43
44 The impressions produced at 0.5 N load and 2.0 N load are exemplified in
45
46 **Figure 12(a)** and **Figure 12(b)**, respectively. In particular, such micrographs were
47
48 acquired on the cross section of the **HAp_2** samples, but analogous indents were
49
50 induced and observed also on the other materials.
51
52
53

54 As shown in **Figure 13(a)**, the micro-hardness of the HAp sintered bodies
55
56 slightly decreases when the applied load rises from 0.5 to 2.0 N, as a result of the well-
57
58
59
60
61
62
63
64
65

1 known Indentation Size Effect (ISE) [25]. The local elastic modulus, instead, is less
2 sensitive to the applied load, especially for the **HAp_1** and **HAp_2** samples, as shown
3 in **Figure 13(b)**. Independently of the applied load, the best local mechanical properties
4 are achieved by the **HAp_2** sintered bodies, a result that is reasonable on the basis of
5 the mineralogical composition and compact microstructure detected for this material, as
6 described in the previous paragraphs. The relatively low mechanical properties observed
7 for the **HAp_1** samples with respect to the other two SPSed HAp materials are probably
8 due to the chemical transformations occurred during sintering and the incomplete
9 densification. However, it is worth noting that, also for the **HAp_1** samples, the
10 hardness is well comparable to that usually reported in the literature for apatites
11 produced with different methods. **Ramesh et al. [26]**, for example, analyze the sintering
12 properties of hydroxyapatite powders obtained with different methods and describe
13 hardness values indicatively in the 50-700 HV range, whereas **Curran et al. [27]**,
14 comparing undoped and Sr-doped sintered HAp samples treated at 1200°C, find values
15 in the 200-500 HV range. Also the local elastic modulus matches the values commonly
16 observed for crystalline apatite solids (e.g. 114 GPa according to the classical study of
17 **Gilmore et al. [28]**).

4. Summary and concluding remarks

47 Three commercially available HAp powders are processed in this work taking
48 advantage of the Spark Plasma Sintering technology to rapidly obtain nearly full dense
49 ceramics.
50

51 The starting powders differences in term of purity, particle size, microstructure,
52 and thermo-chemical stability are found to strongly affect their sintering behavior as
53
54
55
56
57
58
59
60
61
62
63
64
65

1 well as the characteristics of the resulting bulk materials. In particular, a fully dense
2 product with no secondary phases was obtained by SPS at 900°C when using the
3 relatively small sized, with refined grains and high purity **HAp_2** powders. On the other
4 hand, significantly higher temperature levels (1200 °C) are required to eliminate
5 residual porosity in the product when starting from the coarser **HAp_3** powders.
6 Nevertheless, such temperature conditions are not so drastic to induce the formation of
7 undesired phases in this material during its consolidation by SPS. In contrast, a marked
8 decomposition of HAp to β -TCP, which becomes the major phase in the end product,
9 was obtained under the same conditions (1200°C) when processing the **HAp_1** system,
10 whose initial fine powders also contained CaHPO₄.
11
12
13
14
15
16
17
18
19
20
21
22
23
24

25 The optical, microstructural, and mechanical properties of the obtained dense
26 bodies are consistent with the characteristics of the starting material and the
27 corresponding SPS conditions adopted. The system exhibiting relatively higher
28 transparency is **HAp_2** whereas the other specimens, particularly **HAp_1**, appear more
29 opaque. This outcome is important as sample transparency enables direct viewing of
30 living cells during biological characterization by light microscopy of the obtained
31 materials. The achieved samples transparency can be directly associated with the related
32 microstructures. Indeed, a **HAp_2** product consisting of sub-micrometer sized
33 hydroxyapatite grains was obtained after the consolidation process, while relatively
34 coarser microstructures were evidenced in the **HAp_1** and **HAp_3** end products. In
35 addition, the transformation HAp \rightarrow β -TCP occurred during sintering makes **HAp_1**
36 more sensitive to the chemical etching with respect to the other systems where the
37 decomposition above was avoided.
38
39
40
41
42
43
44
45
46
47
48
49
50
51
52
53
54
55
56
57
58
59
60
61
62
63
64
65

1 As far as the mechanical properties of the three HAp materials are concerned, it
2
3 was found that they are well comparable to those ones generally reported in the
4
5 literature for apatite based products fabricated via alternative methods. In particular, the
6
7 best local mechanical properties are achieved by the **HAp_2** materials, whereas
8
9 relatively lower hardness and elastic modulus values were obtained for the **HAp_1**
10
11 samples. The good mechanical characteristics of the **HAp_2** material can be ascribed to
12
13 its thermal stability and finer microstructure. On the other hand, the presence of
14
15 significant amount of β -TCP in the **HAp_1** sintered product is, along with the
16
17 corresponding coarser microstructure, responsible for mechanical properties worsening.
18
19
20
21
22
23
24

25 **Acknowledgements**

26
27 The financial support for this work from Regione Autonoma della Sardegna
28
29 (Italy), L.R. n.7/2007, CUP n. F71J11001070002, is gratefully acknowledged. One of us
30
31 (A.C.) has performed his activity in the framework of the PhD in Biomedical
32
33 Engineering at the University of Cagliari, Italy. The authors thank Dr. Luca Desogus
34
35 (University of Cagliari, Italy) for his valuable support during the experimental activity.
36
37
38
39
40
41
42
43
44
45
46
47
48
49
50
51
52
53
54
55
56
57
58
59
60
61
62
63
64
65

References

- [1] Dorozhkin S.V. Bioceramics of calcium orthophosphates. *Biomaterials* 2010; 31(7): 1465-1485
- [2] Champion E. Sintering of calcium phosphate bioceramics. *Acta Biomater.* 2013; 9(4): 5855-5875
- [3] Bolelli G., Bellucci D., Cannillo V., Lusvarghi L., Sola A., Stiegler N., Müller P., Killinger A., Gadow R., Altomare L., De Nardo L. Suspension thermal spraying of hydroxyapatite: Microstructure and in vitro behaviour. *Mat. Sci. Eng. C* 2014; 34: 287-303.
- [4] Cihlar J., Buchal A., Trunec M. Kinetics of thermal decomposition of hydroxyapatite bioceramics. *J. Mater. Sci.* 1999; 34: 6121–6131
- [5] Orrù R., Licheri R., Locci A.M., Cincotti A., Cao G. Consolidation/synthesis of materials by electric current activated/assisted sintering. *Mat. Sci. Eng. R* 2009; 63(4-6): 127-287.
- [6] Gu Y.W., Loh N.H., Khor K.A., Tor S.B., Cheang P. Spark plasma sintering of hydroxyapatite powders. *Biomaterials* 2002; 23(1): 37-43
- [7] Nakahira A., Tamai M., Aritani H., Nakamura S., Yamashita K. Biocompatibility of dense hydroxyapatite prepared using an SPS process. *J. Biomed. Mater. Res.* 2002; 62(4): 550-557.
- [8] Kumar R., Cheang P., Khor K.A. Spark plasma sintering and in vitro study of ultra-fine HA and ZrO₂-HA powders. *J. Mater. Process. Technol.* 2003; 140: 420-425
- [9] Watanabe Y., Ikoma T., Monkawa A., Suetsugu Y., Yamada H., Tanaka J., Moriyoshi Y. Fabrication of transparent hydroxyapatite sintered body with high

- 1 crystal orientation by pulse electric current sintering. J. Amer. Ceram. Soc. 2005;
2
3 88(1): 243-245
4
5
6 [10] Guo X., Xiao P., Liu J., Shen Z. Fabrication of nanostructured hydroxyapatite via
7
8 hydrothermal synthesis and spark plasma sintering. J. Amer. Ceram. Soc. 2005;
9 88: 1026-1029
10
11
12 [11] Lee B.T., Shin N.Y., Han J.K., Song H.Y. Microstructures and fracture
13 characteristics of spark plasma-sintered HAp-5 vol.% Ag composites. Mat. Sci.
14 Eng. A 2006; 429(1-2): 348-352
15
16
17 [12] Omori M., Onoki T., Hashida T., Okubo A., Murakami Y. Low temperature
18 synthesis of hydroxyapatite from $\text{CaHPO}_4 \cdot 2\text{H}_2\text{O}$ and $\text{Ca}(\text{OH})_2$ based on effect of
19 the spark plasma system (SPS). Ceram. Int. 2006; 32(6): 617-621
20
21
22 [13] Guo X., Gough J.E., Xiao P., Liu J., Shen Z. Fabrication of nanostructured
23 hydroxyapatite and analysis of human osteoblastic cellular response. J Biomed
24 Mater Res A. 2007; 82(4):1022-1032.
25
26
27 [14] Li H., Khor K.A., Chow V., Cheang P. Nanostructural characteristics, mechanical
28 properties, and osteoblast response of spark plasma sintered hydroxyapatite. J
29 Biomed Mater Res A. 2007; 82(2): 296-303.
30
31
32 [15] Xu J.L., Khor K.A., Kumar R. Physicochemical differences after densifying radio
33 frequency plasma sprayed hydroxyapatite powders using spark plasma and
34 conventional sintering techniques. Mat. Sci. Eng. A 2007; 457(1-2): 24-32
35
36
37 [16] Gandhi A.A., Gunning R.D., Ryan K.M., Tofail S.A.M. The role of texturing and
38 densification on optical transmittance of hydroxyapatite ceramics. J. Amer.
39 Ceram. Soc. 2010; 93(11): 3773-3777.
40
41
42
43
44
45
46
47
48
49
50
51
52
53
54
55
56
57
58
59
60
61
62
63
64
65

- 1 [17] Eriksson M., Liu Y., Hu J., Gao L., Nygren M., Shen Z. Transparent
2 hydroxyapatite ceramics with nanograin structure prepared by high pressure spark
3 plasma sintering at the minimized sintering temperature. *J. Eur. Ceram. Soc.*
4 2011; 31 (9): 1533-1540
5
6
7
8
9
10 [18] Liu Y., Shen Z. Dehydroxylation of hydroxyapatite in dense bulk ceramics
11 sintered by spark plasma sintering. *J. Eur. Ceram. Soc.* 2012; 32(11): 2691-2696.
12
13 [19] Kim B.N., Prajatelista E., Han Y.H., Son H.W., Sakka Y., Kim S. Transparent
14 hydroxyapatite ceramics consolidated by spark plasma sintering *Scripta Mater.*
15 2013; 69(5): 366-369
16
17
18 [20] Locci A.M., Orrù R., Cao G., Munir Z.A. Effect of ball milling on simultaneous
19 spark plasma synthesis and densification of TiC-TiB₂ composites. *Mat. Sci. Eng.*
20 *A* 2006; 434(1-2): 23-29.
21
22 [21] Oliver W.C., Pharr G.M. An Improved Technique for Determining Hardness and
23 Elastic Modulus using Load and Displacement Sensing Indentation Experiments.
24 *J. Mater. Res.* 1992; 7(6): 1564-1583.
25
26 [22] Liao, C.-J., Lin, F.-H., Chen, K.-S., Sun, J.-S. Thermal decomposition and
27 reconstitution of hydroxyapatite in air atmosphere. *Biomaterials* 1999; 20(19):
28 1807-1813.
29
30 [23] Raynaud, S., Champion, E., Bernache-Assollant, D., Thomas, P. Calcium
31 phosphate apatites with variable Ca/P atomic ratio I. Synthesis, characterisation
32 and thermal stability of powders. *Biomaterials* 2002; 23(4): 1065-1072.
33
34 [24] Graeve, O.A., Kanakala, R., Madadi, A., Williams, B.C., Glass, K.C.
35 Luminescence variations in hydroxyapatites doped with Eu²⁺ and Eu³⁺ ions.
36 *Biomaterials* 2010; 31(15): 4259-4267
37
38
39
40
41
42
43
44
45
46
47
48
49
50
51
52
53
54
55
56
57
58
59
60
61
62
63
64
65

- 1 [25] Milman Yu.V., Golubenko A.A., Dub S.N. Indentation size effect in
2 nanohardness. *Acta Mater.* 2011; 59(20): 7480-7487.
3
4
5
6 [26] Ramesh S., Aw K.L., Tolouei R., Amiriyan M., Tan C.Y., Hamdi M.,
7 Purbolaksono J., Hassan M.A., Teng W.D. Sintering properties of hydroxyapatite
8 powders prepared using different methods. *Ceram. Int.* 2013; 39: 111-119.
9
10
11
12
13 [27] Curran D.J., Fleming T.J., Towler M.R., Hampshire S. Mechanical parameters of
14 strontium doped hydroxyapatite sintered using microwave and conventional
15 methods. *J. Mech. Behav. Biomed. Mater.* 2011; 4(8): 2063-2073.
16
17
18
19
20 [28] Gilmore R.S., Katz J.L. Elastic properties of apatites. *J. Mater. Sci.* 1982; 17(4):
21 1131-1141.
22
23
24
25
26
27
28
29
30
31
32
33
34
35
36
37
38
39
40
41
42
43
44
45
46
47
48
49
50
51
52
53
54
55
56
57
58
59
60
61
62
63
64
65

Table 1. Starting powders characteristics as provided by suppliers.

System ID	Supplier/Code	Particle size (μm)	Compositional details
HAp_1	Sigma-Aldrich Cod. 21223	25-45 (average)	$\geq 90\%$ purity (KT as $\text{Ca}_3(\text{PO}_4)_2$)
HAp_2	Alfa-Aesar Cod. 36731	< 44	Calcium phosphate tribasic, 38.1% Ca
HAp_3	Plasma Biotol Ltd Cod. CAPTAL 60-1	$d_{10} = 21.7$ $d_{50} = 43$ $d_{90} = 77.8$	Hydroxyapatite, Whitlockite ($< 1\%$)

Table 2. Particle size characteristics of starting powders as determined by laser light scattering analyser.

System ID	d_{10} (μm)	d_{50} (μm)	d_{90} (μm)	Average size (μm)
HAp_1	1.2	4.9	17.2	7.1
HAp_2	1.3	5.1	13.4	6.3
HAp_3	8.8	34.0	52.0	32.7

Captions for figures

1 **Figure 1.** SEM images at different magnitudes of the initial HAp powders used in the present
2 investigation: (a)-(b) **HAp_1**, (c)-(d) **HAp_2** and (e)-(f) **HAp_3**.
3

4 **Figure 2.** XRD patterns on the initial HAp powders used in the present work: (a) **HAp_1**, (b)
5 **HAp_2** and (c) **HAp_3**.
6

7 **Figure 3.** Effect of the heat treatment in air on the composition of (a) **HAp_1**, (b) **HAp_2** and (c)
8 **HAp_3** powders.
9

10 **Figure 4.** Mass loss of HAp powders during TGA in air.
11

12 **Figure 5.** Compositional changes of (a) **HAp_1**, (b) **HAp_2** and (c) **HAp_3** powders during TGA
13 (10°C/min) in air (100 ml/min).
14

15 **Figure 6.** Temperature and sample shrinkage time profiles recorded during consolidation of
16 **HAp_2** powders by SPS (900°C, 75 °C/min, $t_D=5$ min, 30 MPa).
17

18 **Figure 7.** Influence of the sintering temperature on the density of the HAp products obtained by
19 SPS (75 °C/min, $t_D=5$ min, 30 MPa).
20

21 **Figure 8.** Comparison of XRD patterns before and after consolidation by SPS (75 °C/min, $t_D=5$
22 min, 30 MPa) of (a) **HAp_1**, (b) **HAp_2** and (c) **HAp_3** powders.
23

24 **Figure 9.** Temporal evolution of gas pressure during the SPS process (75 °C/min, $t_D=5$ min, 30
25 MPa) of **HAp_1**, **HAp_2** and **HAp_3** powders.
26

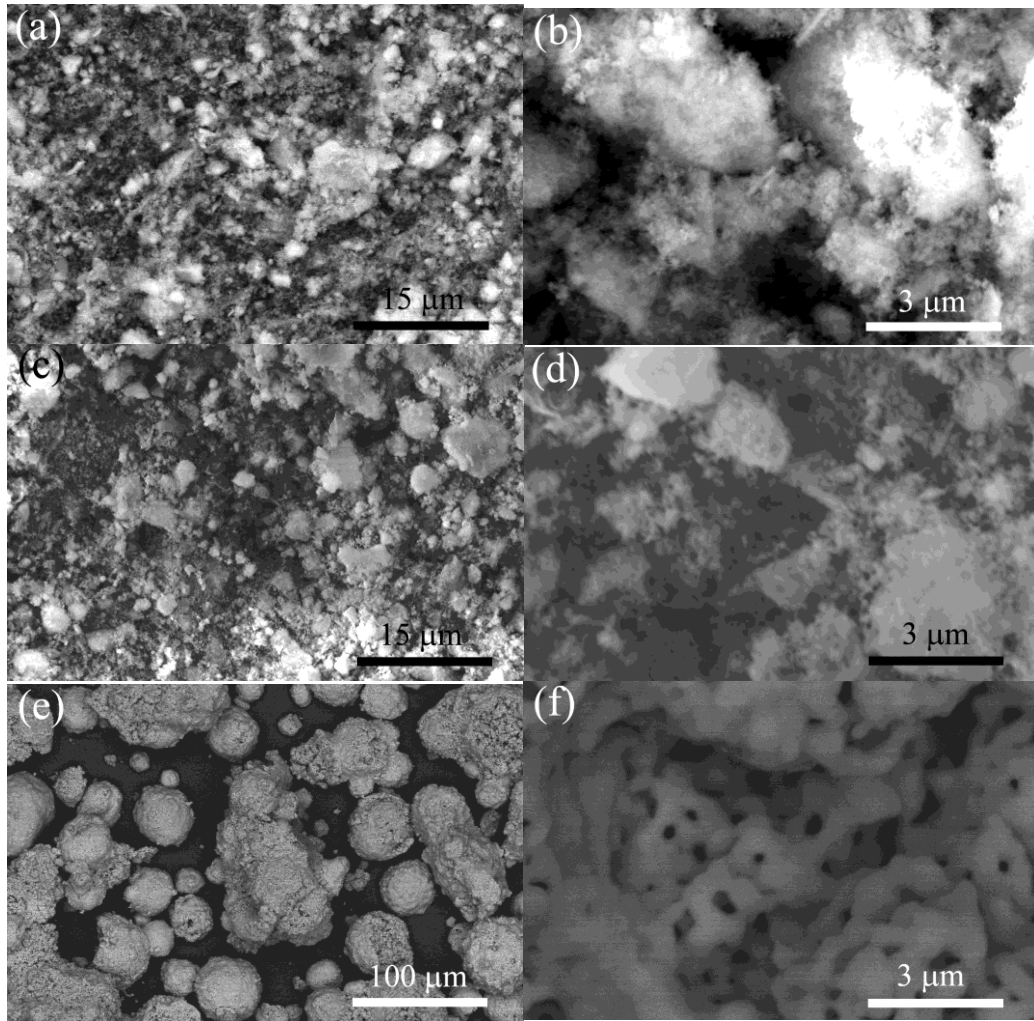
27 **Figure 10.** SEM micrographs (10000 x) of chemically etched dense products obtained by SPS
28 under optimal conditions: (a) **HAp_1**, (b) **HAp_2** and (c) **HAp_3**.
29

30 **Figure 11.** Optical photographs of dense products obtained by SPS under optimal conditions: (a)
31 **HAp_1**, (b) **HAp_2** and (c) **HAp_3**.
32

33 **Figure 12.** Residual imprints produced in the cross section of the **HAp_2** samples during
34 indentation tests: (a) 0.5 N and 2.0 N (b) loads.
35

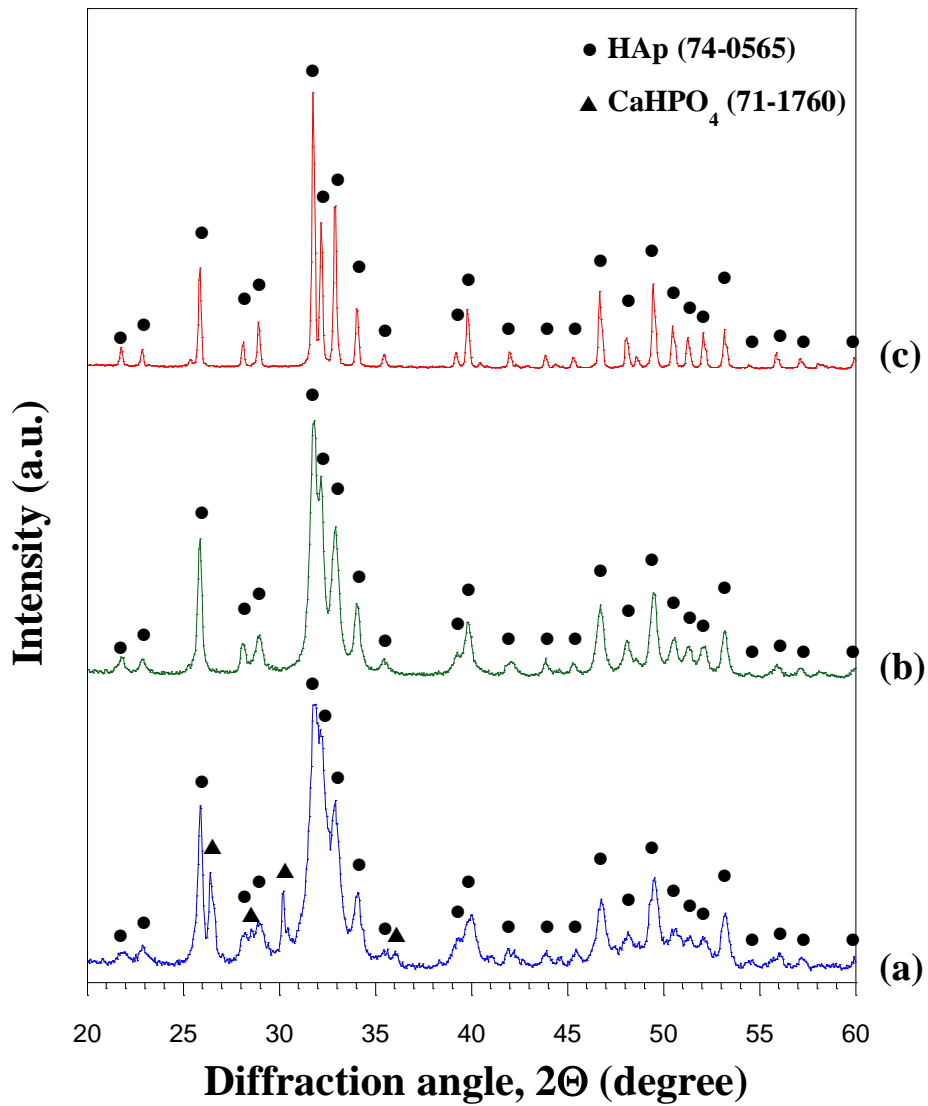
36 **Figure 13.** Mechanical test results performed on **HAp_1**, **HAp_2** and **HAp_3** materials obtained
37 by SPS under optimal sintering conditions: (a) micro-hardness and (b) local elastic
38 modulus.
39
40
41
42
43
44
45
46
47
48
49
50
51
52
53
54
55
56
57
58
59
60
61
62
63
64
65

Figure 1. SEM images at different magnitudes of the initial HAp powders used in the present investigation: (a)-(b) **HAp_1**, (c)-(d) **HAp_2** and (e)-(f) **HAp_3**.



1
2
3
4
5
6
7
8
9
10
11
12
13
14
15
16
17
18
19
20
21
22
23
24
25
26
27
28
29
30
31
32
33
34
35
36
37
38
39
40
41
42
43
44
45
46
47
48
49
50
51
52
53
54
55
56
57
58
59
60
61
62
63
64
65

Figure 2. XRD patterns on the initial HAp powders used in the present work: (a) HAp_1, (b) HAp_2 and (c) HAp_3.



1
2
3
4
5
6
7
8
9
10
11
12
13
14
15
16
17
18
19
20
21
22
23
24
25
26
27
28
29
30
31
32
33
34
35
36
37
38
39
40
41
42
43
44
45
46
47
48
49
50
51
52
53
54
55
56
57
58
59
60
61
62
63
64
65

Figure 3. Effect of the heat treatment in air on the composition of (a) **HAp_1**, (b) **HAp_2** and (c) **HAp_3** powders.

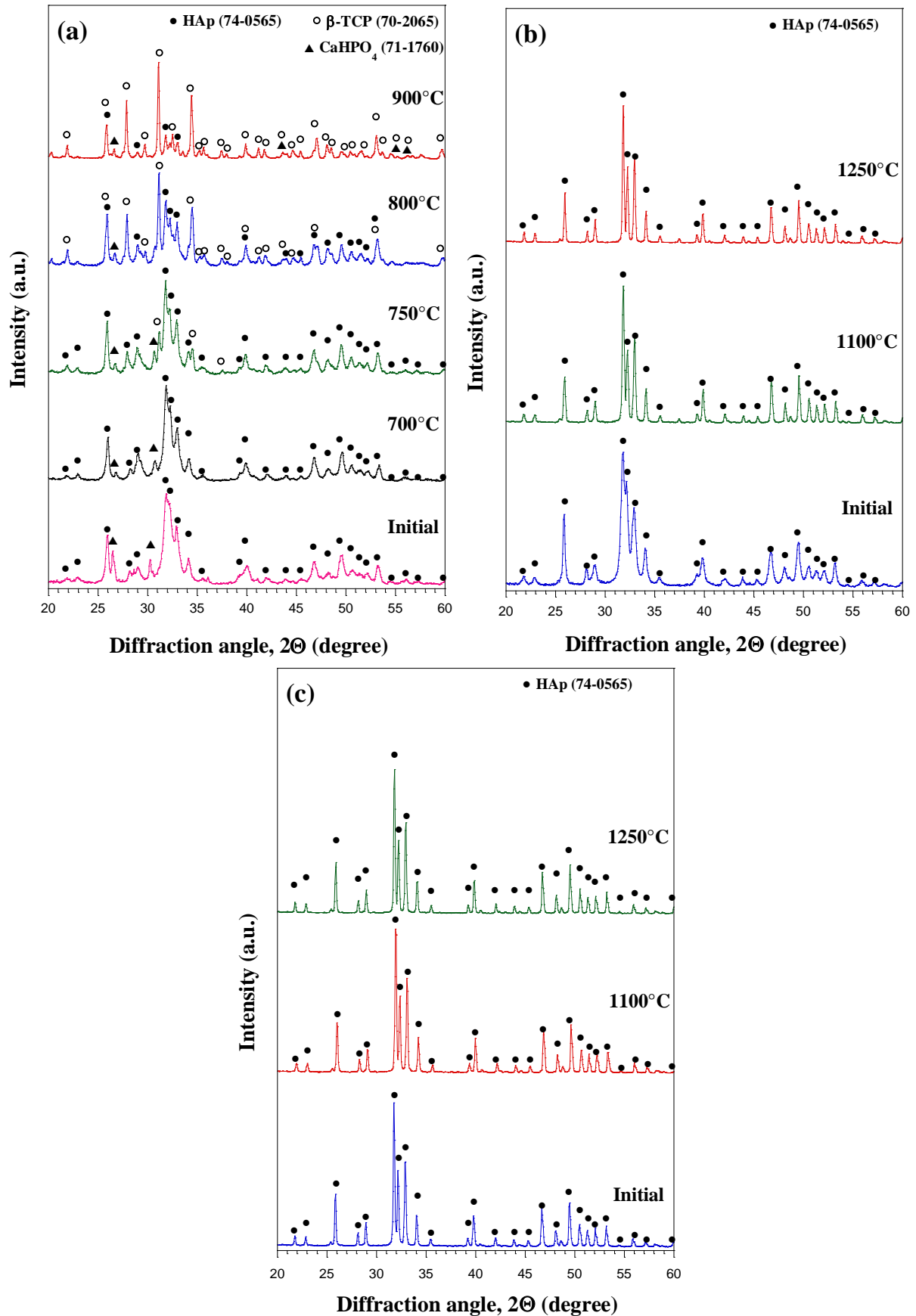
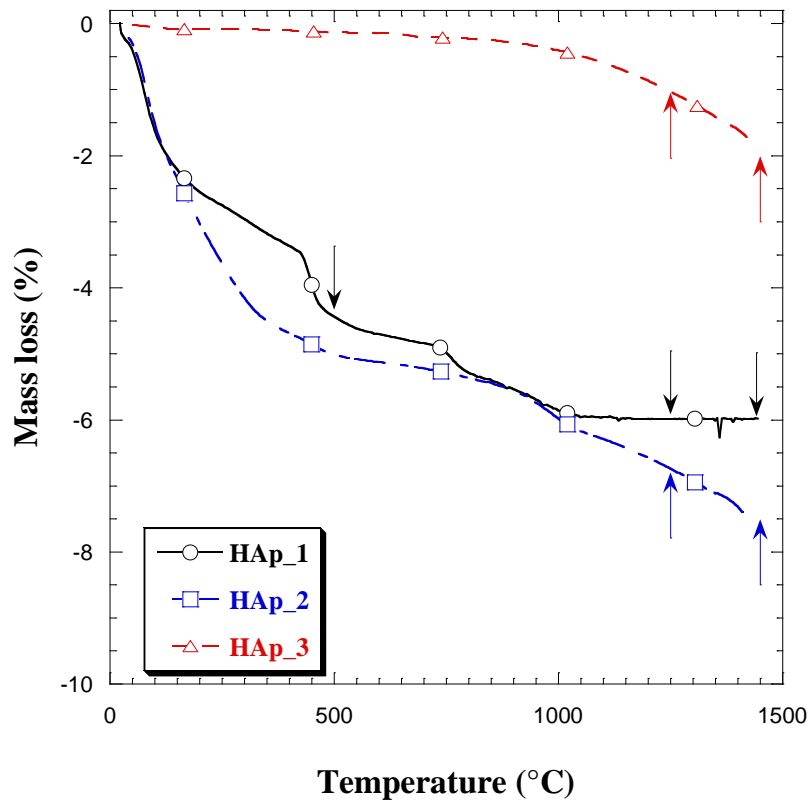


Figure 4. Mass loss of HAp powders during TGA in air.



1
2
3
4
5
6
7
8
9
10
11
12
13
14
15
16
17
18
19
20
21
22
23
24
25
26
27
28
29
30
31
32
33
34
35
36
37
38
39
40
41
42
43
44
45
46
47
48
49
50
51
52
53
54
55
56
57
58
59
60
61
62
63
64
65

Figure 5. Compositional changes of (a) **HAp_1**, (b) **HAp_2** and (c) **HAp_3** powders during TGA (10°C/min) in air (100 ml/min) (cf. **Figure 4**).

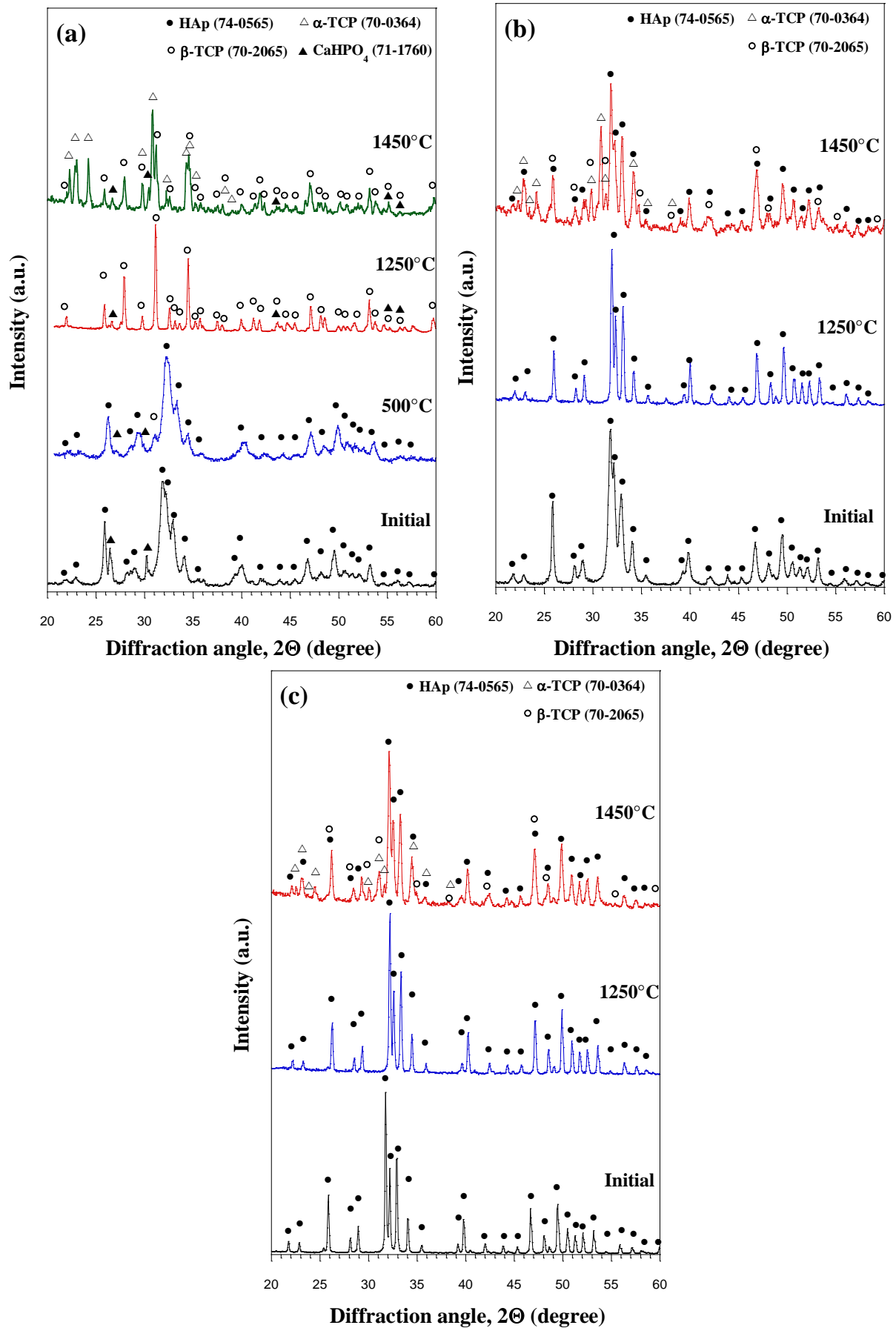
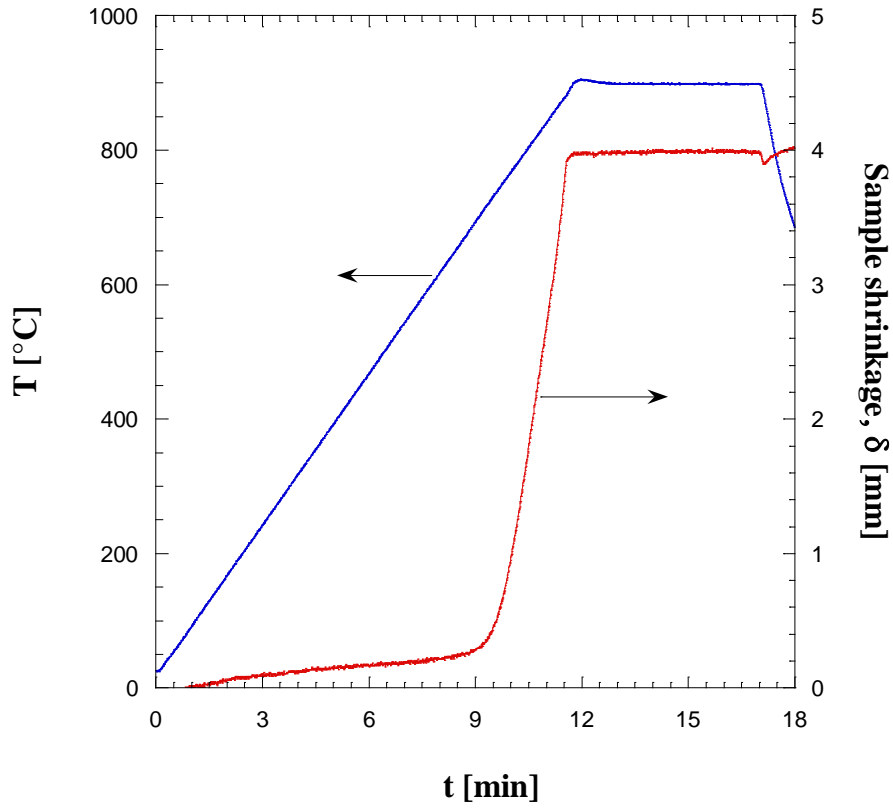
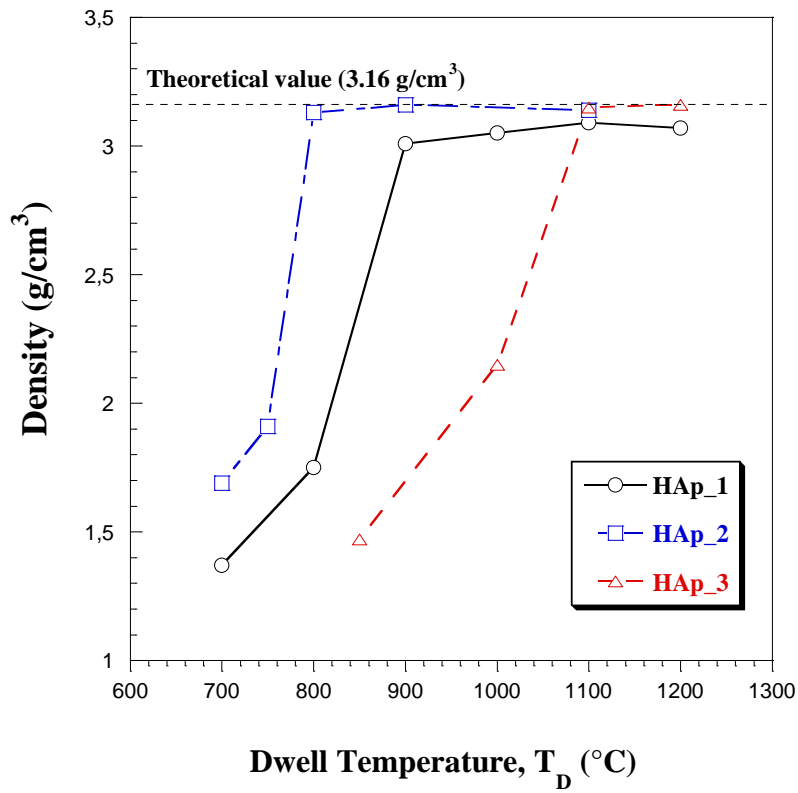


Figure 6. Temperature and sample shrinkage time profiles recorded during consolidation of **HAp_2** powders by SPS (900°C, 75 °C/min, $t_D=5$ min, 30 MPa).



1
2
3
4
5
6
7
8
9
10
11
12
13
14
15
16
17
18
19
20
21
22
23
24
25
26
27
28
29
30
31
32
33
34
35
36
37
38
39
40
41
42
43
44
45
46
47
48
49
50
51
52
53
54
55
56
57
58
59
60
61
62
63
64
65

Figure 7. Influence of the sintering temperature on the density of the HAp products obtained by SPS (75 °C/min, $t_D=5$ min, 30 MPa).



1
2
3
4
5
6
7
8
9
10
11
12
13
14
15
16
17
18
19
20
21
22
23
24
25
26
27
28
29
30
31
32
33
34
35
36
37
38
39
40
41
42
43
44
45
46
47
48
49
50
51
52
53
54
55
56
57
58
59
60
61
62
63
64
65

Figure 8. Comparison of XRD patterns before and after consolidation by SPS (75 °C/min, $t_D=5$ min, 30 MPa) of (a) **HAp_1**, (b) **HAp_2** and (c) **HAp_3** powders.

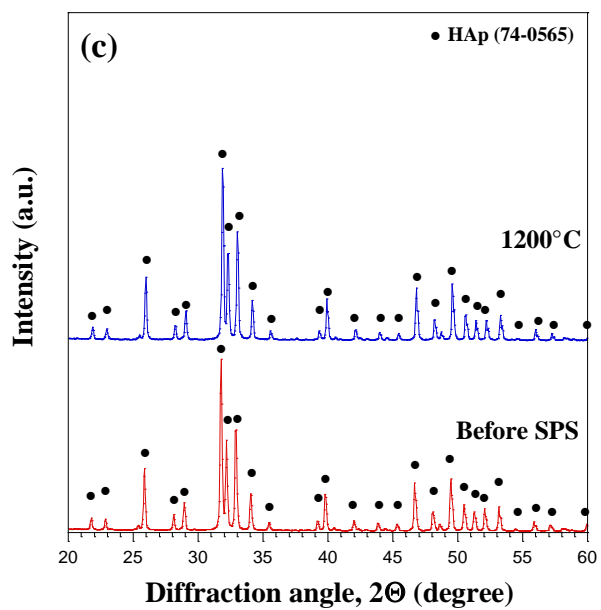
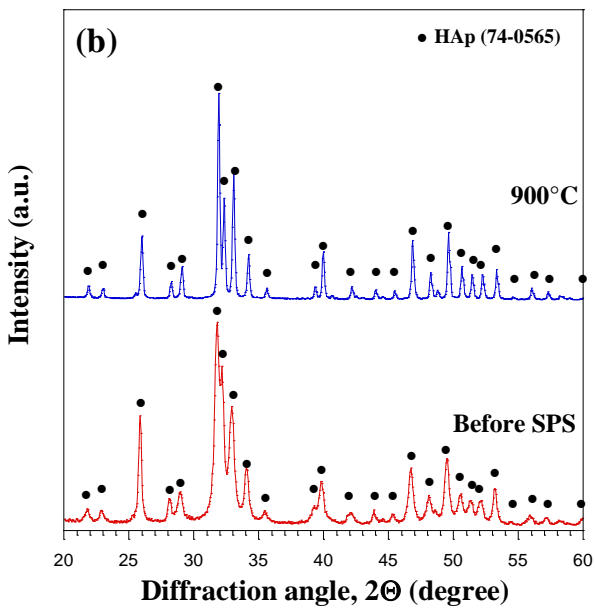
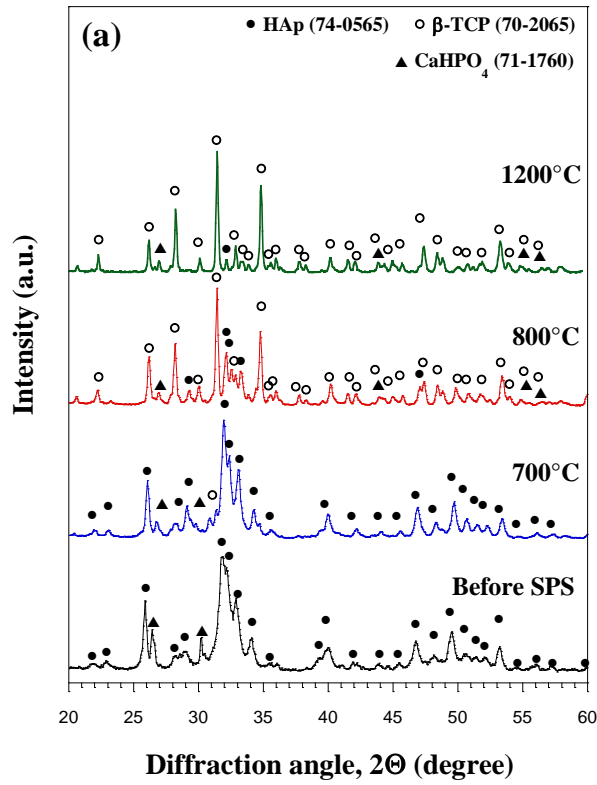
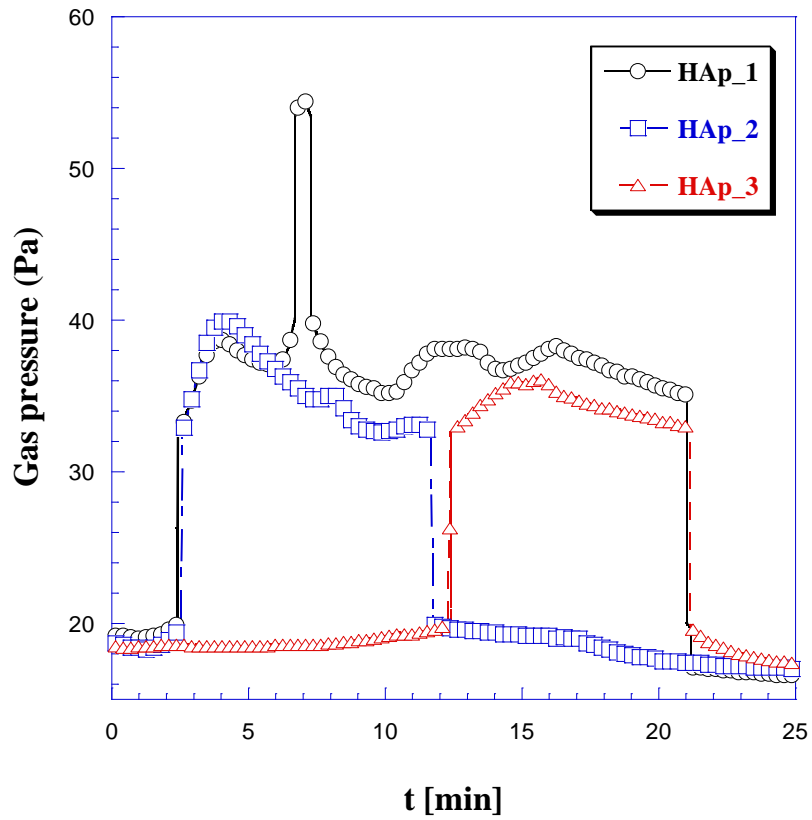


Figure 9. Temporal evolution of gas pressure during the SPS process ($75\text{ }^{\circ}\text{C}/\text{min}$, $t_D=5\text{ min}$, 30 MPa) of **HAp_1**, **HAp_2** and **HAp_3** powders.



1
2
3
4
5
6
7
8
9
10
11
12
13
14
15
16
17
18
19
20
21
22
23
24
25
26
27
28
29
30
31
32
33
34
35
36
37
38
39
40
41
42
43
44
45
46
47
48
49
50
51
52
53
54
55
56
57
58
59
60
61
62
63
64
65

Figure 10. SEM micrographs (5000x) of chemically etched dense products obtained by SPS under optimal conditions: (a) **HAp_1**, (b) **HAp_2** and (c) **HAp_3**.

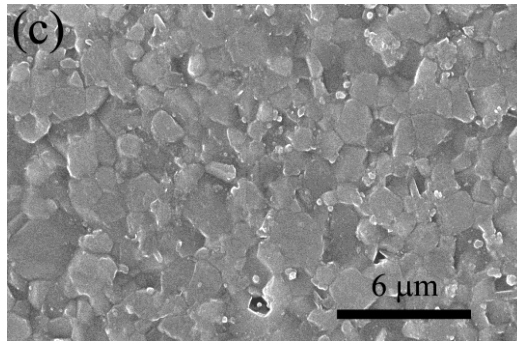
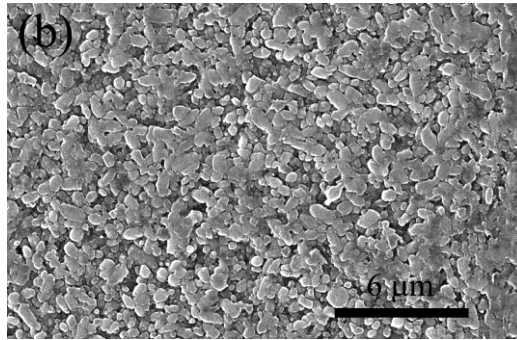
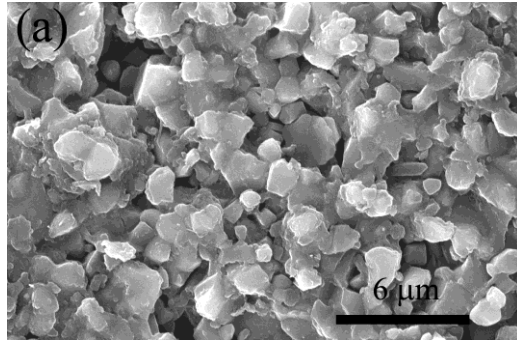
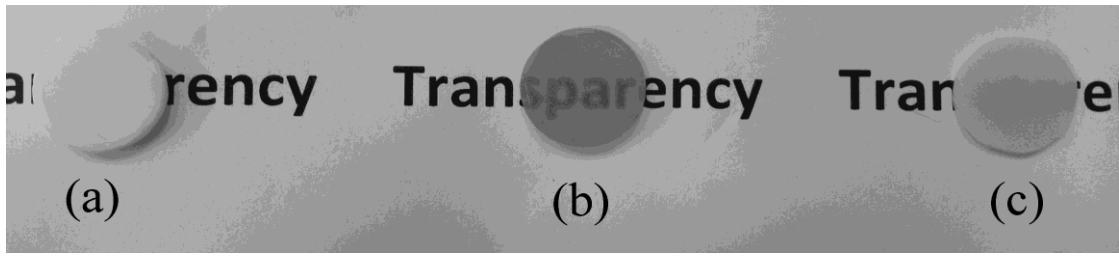


Figure 11. Optical photographs of dense products obtained by SPS under optimal conditions: (a) **HAp_1**, (b) **HAp_2** and (c) **HAp_3**.



1
2
3
4
5
6
7
8
9
10
11
12
13
14
15
16
17
18
19
20
21
22
23
24
25
26
27
28
29
30
31
32
33
34
35
36
37
38
39
40
41
42
43
44
45
46
47
48
49
50
51
52
53
54
55
56
57
58
59
60
61
62
63
64
65

Figure 12. Residual imprints produced in the cross section of the **HAp_2** samples during indentation tests: (a) 0.5 N and 2.0 N (b) loads.

1
2
3
4
5
6
7
8
9
10
11
12
13
14
15
16
17
18
19
20
21
22
23
24
25
26
27
28
29
30
31
32
33
34
35
36
37
38
39
40
41
42
43
44
45
46
47
48
49
50
51
52
53
54
55
56
57
58
59
60
61
62
63
64
65

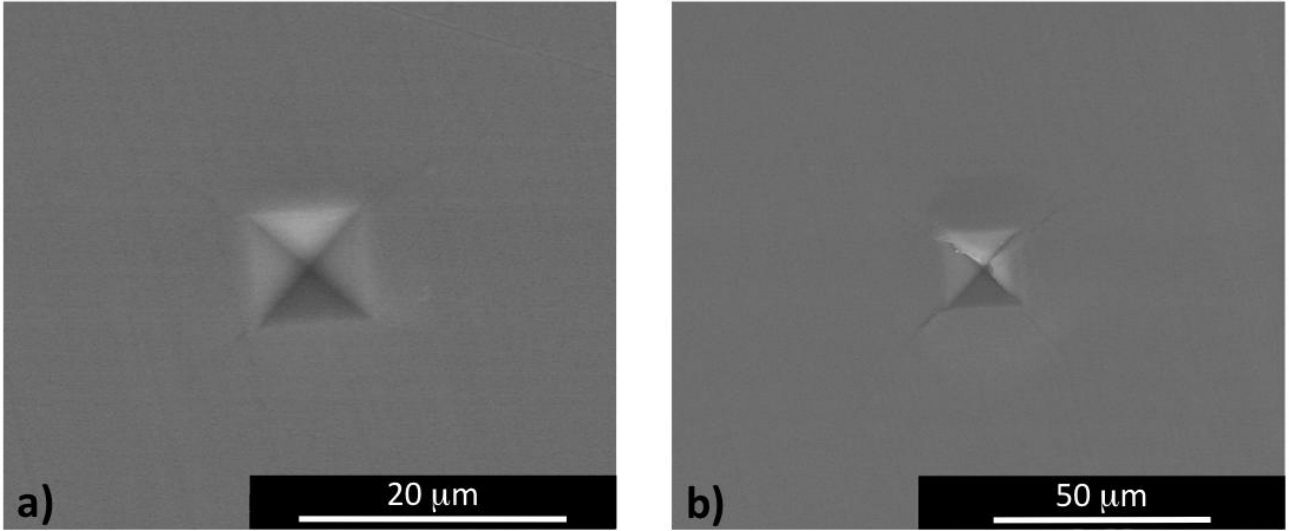
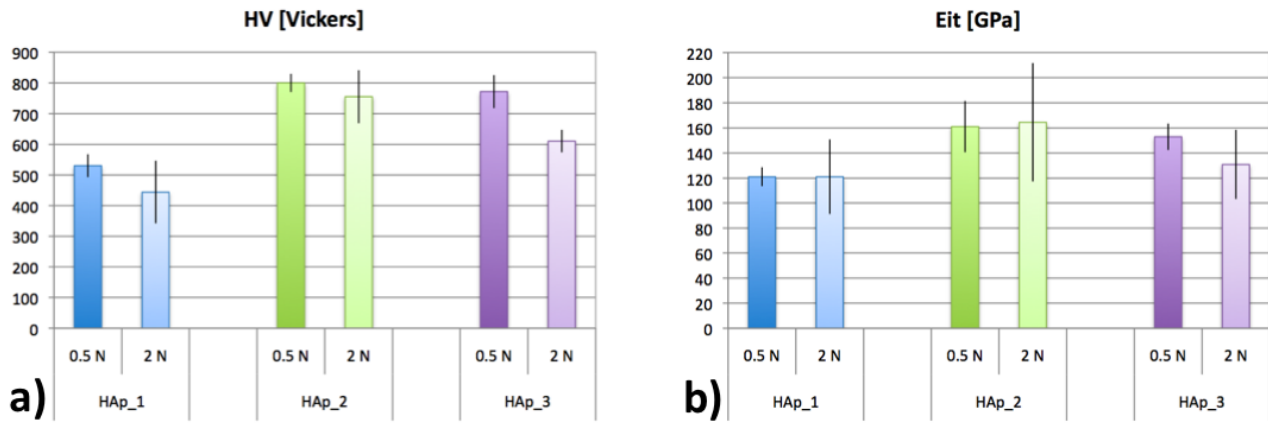


Figure 13. Mechanical test results performed on **HAp_1**, **HAp_2** and **HAp_3** materials obtained by SPS under optimal sintering conditions: (a) micro-hardness and (b) local elastic modulus.



1
2
3
4
5
6
7
8
9
10
11
12
13
14
15
16
17
18
19
20
21
22
23
24
25
26
27
28
29
30
31
32
33
34
35
36
37
38
39
40
41
42
43
44
45
46
47
48
49
50
51
52
53
54
55
56
57
58
59
60
61
62
63
64
65